Nature Communications

https://doi.org/10.1038/s41467-026-70131-w

Article in Press

Phytochrome B integrates jasmonic acid and warm temperature signaling pathways to regulate cotyledon chloroplast development

Received: 28 July 2025

Accepted: 19 February 2026

Cite this article as: Qi, P., Huai, J., Gao, N. *et al.* Phytochrome B integrates jasmonic acid and warm temperature signaling pathways to regulate cotyledon chloroplast development. *Nat Commun* (2026). https://doi.org/10.1038/s41467-026-70131-w

Peipei Qi, Junling Huai, Nan Gao, Yuanyuan Yao & Rongcheng Lin

Phytochrome B integrates jasmonic acid and warm temperature signaling pathways to regulate cotyledon chloroplast development

Peipei Qi[1,2†], Junling Huai[1,3†*], Nan Gao[1], Yuanyuan Yao[1,3], Rongcheng Lin[1,2*]

[1] State Key Laboratory of Forage Breeding-by-Design and Utilization, Laboratory of Photobiology, Institute of Botany, Chinese Academy of Sciences, Beijing 100093, China

[2] Biotechnology Institute, Xianghu Laboratory, Hangzhou 311231, China

[3] University of Chinese Academy of Sciences, Beijing 100049, China

[†] These authors contribute equally to this work.

* Correspondence: Junling Huai (huaijl@ibcas.ac.cn) and Rongcheng Lin (linrongcheng@xhlab.ac.cn; Dr. Lin is fully responsible for the distributions of all materials associated with this article)

Short title: Warm temperature and JA signaling cross-talk

Abstract

Chloroplast biogenesis and development are coordinated by both endogenous factors and environmental cues. The interplay between jasmonic acid (JA) and temperature in regulating chloroplast development remains poorly understood. Here, we demonstrate that methyl jasmonate (MeJA) and warm temperature (28℃) treatments additively impair chlorophyll accumulation and chloroplast development in *Arabidopsis thaliana* cotyledons. We found that the thermosensor phytochrome B (phyB) suppresses, whereas the JA receptor CORONATINE INSENSITIVE 1 (COI1) promotes, MeJA- and warm temperature-mediated chloroplast development. Moreover, phyB directly interacts with JASMONATE ZIM-DOMAIN 1 (JAZ1) and JAZ3, preventing their JA-induced degradation, and warm temperature attenuates this interaction. Strikingly, we reveal that transcription factors ELONGATED HYPOCOTYL 5 (HY5) and MYC2 oppositely regulate cotyledon chloroplast development in response to MeJA and warm temperature by directly and differentially modulating downstream transcriptional networks. Our study establishes a molecular framework in which phyB integrates JA and warm temperature signaling through the HY5-MYCs transcriptional regulatory network to fine-tune chloroplast development, highlighting a plant strategy for ecological adaptation.

Keywords: chloroplast development, temperature, JA, phyB

Introduction

Global climate change poses a threat to world agriculture (Lobell et al., 2011). Modeling suggests that every 1 ℃ increase in global temperature could reduce the yield of major crops by 3-8% (Zhao et al., 2017). Plants have evolved sophisticated sensory and signaling networks to perceive and integrate environmental stimuli, such as light and temperature, to optimize growth and development. Non-stressful warm temperatures profoundly reshape plant development, accelerating phenological transitions like flowering and leaf senescence, and promoting hypocotyl and petiole elongation, a process termed thermomorphogenesis (Quint et al., 2016; Casal and Balasubramanian, 2019). Phytochrome B (phyB) functions as both a dominant red-light photoreceptor and a thermosensor that triggers light and warm temperature signaling pathways (Li et al., 2011; Casal and Balasubramanian, 2019). PhyB exists in two photoconvertible conformations: the red light-absorbing inactive Pr form and the far-red light-absorbing active Pfr form. Upon light activation, the Pfr form of phyB translocates to the nucleus, where it interacts with PHYTOCHROME-INTERACTING FACTORs (PIFs) to regulate downstream gene expression (Leivar and Quail, 2011). phyB also undergoes light-independent Pfr-to-Pr dynamic thermal reversion and the relative amount of the Pr form is accelerated with increasing temperature (Klose et al., 2020). A recent study revealed that while light induces phyB photobody formation, the N-terminal extension of phyB acts as a biophysical modulator of phase separation to directly sense warm temperature (Chen et al., 2022). This temperature-dependent thermal reversion provides the molecular basis for phyB to function as a thermosensor controlling plant elongation growth (Jung et al., 2016; Legris et al., 2016). PIF4 serves as a transcriptional hub in the warm temperature signaling pathway, with warm temperature enhancing both *PIF4* transcription and PIF4 protein stability (Koini et al., 2009; Foreman et al., 2011; Kim et al., 2020). Some studies also indicate that an effect of elevated temperature on cotyledon and leaf morphology. For example, PIF4 and PIF5 are required for warm temperature-induced leaf senescence, as their double mutant retains more chlorophyll than wild-type seedlings (Kim et al., 2020).

Jasmonic acid (JA) is a phytohormone that regulates plant growth and defense against abiotic stresses (Hong et al., 2024). The canonical JA signaling pathway comprises the receptor (CORONATINE INSENSITIVE 1, COI1), repressors of the JASMONATE ZIM-DOMAIN (JAZ) family, and downstream transcription factors/regulators (Li et al., 2022a). Under normal conditions, endogenous bioactive JAs are maintained at a low basal level. Upon environmental or developmental stimulation, the F-box protein COI1 recruits JAZ proteins for ubiquitination and degradation via the 26S proteasome pathway, thereby releasing downstream transcription factors to activate JA responses (Xu et al., 2002; Chini et al., 2007; Fernandez-Calvo et al., 2011; Wang et al., 2021; Hu et al., 2023). JA signaling also inhibits growth and promotes senescence, reflecting the classic trade-off between growth and defense (Li et al., 2022a). Previous studies indicate that the basic helix-loop-helix (bHLH) transcription factors MYC2, MYC3, and MYC4 may mediate JA-induced chlorophyll degradation by directly activating chlorophyll catabolic genes (Zhu et al., 2015). Following JA treatment, the *myc2/3/4* triple mutant exhibits a stay-green phenotype with high chlorophyll content, similar to the *coi1-1* mutant. In contrast, lines overexpressing *MYC*s display precocious leaf senescence, supporting a role for JA in promoting chloroplast maturation (Qi et al., 2015; Zhu et al., 2015). Additionally, JA activates a subset of senescence-associated genes (*SAGs*) to promote leaf senescence. MYC2/MYC3/MYC4 activate the expression of *SAG29* to enhance JA-induced leaf senescence, whereas several other bHLH transcription factors bind to the *SAG29* promoter and repress its MYCs-activated expression (Qi et al., 2015).

Several previous studies have revealed connections between warm temperature and JA signaling. Warm temperature can upregulate the expression of *Jasmonate Oxidases* and *Sulfotransferase Family 2A* (*ST2A*) to regulate jasmonate catabolism (Zhu et al., 2021). The resulting reduction in bioactive JA levels stabilizes JAZ proteins, thereby ultimately promoting plant growth in warm temperature (Zhu et al., 2021). Similarly, neighbor competition promotes plant growth by upregulating *ST2A* to reduce bioactive JA levels, a process mediated through the phyB-PIF module (Fernandez-Milmanda et al., 2020).

While the majority of thermomorphogenesis studies have focused on hypocotyl and stem elongation, this study investigates cotyledon and chloroplast development. We found that warm temperature and JA additively induce cotyledon chlorosis. We demonstrate that phyB interacts with JAZ1 and JAZ3 and enhances their protein stability. Furthermore, we show that HY5 and MYC2 oppositely regulate downstream gene expression and, subsequently, JA- and warm temperature-mediated chloroplast development in the cotyledons. Our findings reveal a previously uncharacterized crosstalk between JA and warm temperature signaling pathways in regulating seedling development.

Results

JA and warm temperature additively regulate chlorophyll accumulation and chloroplast development in cotyledons

To establish a cotyledon-based experimental system, Columbia-0 (Col-0) wild-type seedlings of *Arabidopsis thaliana* were grown on Murashige and Skoog medium (MS) supplemented with or without methyl jasmonate (MeJA, a JA derivative) under continuous white light at temperatures ranging from 18℃ to 30℃ for 6 days. Both 25 μM and 50 μM of MeJA treatments significantly reduced the chlorophyll content in the cotyledons, and increasing temperature enhanced the chlorosis phenotype induced by MeJA (Supplementary Fig. 1). In the subsequent experiments, we examined the physiological responses by growing seedlings on MS medium in the absence (mock) or presence of 25 μM MeJA at 22℃ (normal growth temperature) and 28℃ (warm temperature). These four conditions were designated as 22℃, 22℃+MeJA, 28℃, and 28℃+MeJA (Fig. 1a).

We found that MeJA treatment at 22℃ reduced cotyledon size, chlorophyll content, maximum quantum yield of photosystem II (Fv/Fm), effective quantum yield of photosystem II (ΦPSII), electron transport rate (ETR), and qP (coefficient of photochemical quenching). The combined 28℃+MeJA treatment further significantly enhanced these effects compared to the other three conditions (Fig. 1b-e; Supplementary Fig. 2). These changes in photosynthetic fluorescence prompted us to further investigate their impact on chloroplast development. We subsequently

examined chloroplast morphology using confocal microscope and thylakoid ultrastructure via transmission electron microscopy (Fig. 1f, g). Although the number of chloroplasts per cell did not differ substantially among the four conditions (Fig. 1h), chloroplast size, chlorophyll fluorescence intensity, and the number of stacked thylakoids per granum were markedly reduced under 22℃+MeJA and 28℃ compared to 22℃ alone. These parameters showed further significant reductions under 28℃+MeJA condition (Fig. 1i-k). Collectively, these results demonstrate that JA and warm temperature act additively to impair chlorophyll accumulation and chloroplast development in the cotyledons.

phyB and COI1 play antagonistic roles in JA/warm temperature-mediated cotyledon chloroplast development

Given that COI1 and phyB act as the JA receptor and a thermosensor, respectively, we investigated their roles by examining loss-of-function mutants (*coi1-8* and *phyB-9*) and overexpressing lines (*35S:COI1-GFP* and *35S:Myc-phyB*) under the four experimental conditions. We found that *coi1-8* mutant seedlings were insensitive to MeJA and warm temperature, retaining relatively green cotyledons, higher chlorophyll levels, higher Fv/Fm, ΦPSII, and qP compared to Col-0 under the 28℃+MeJA condition, whereas *35S:COI1-GFP* plants were largely similar to the wild type (Fig. 2a-d; Supplementary Fig. 3a-d). Although *phyB-9* seedlings exhibited smaller cotyledons than the other genotypes (Supplementary Fig. 3a), they displayed opposite phenotype to *coi1-8* at 28℃+MeJA (Fig. 2a-d; Supplementary Fig. 3b-d). In contrast, *35S:Myc-phyB* seedlings showed greener cotyledons with slightly increased Fv/Fm relative to Col-0 (Fig. 2a-d). Consistent with these observations, *coi1-8* and *35S:Myc-phyB* lines exhibited significantly larger chloroplast area and stronger chlorophyll autofluorescence compared to Col-0, whereas *phyB-9* and *35S:COI1-GFP* lines displayed opposite phenotypes under the 28℃+MeJA condition (Fig. 2e-h). Additionally, *coi1-8* mutants had a greater number of chloroplast per cell than Col-0 at 28℃+MeJA (Fig. 2g).

Since phyB also functions as a classical red-light photoreceptor, we further examined the seedling phenotype under red light. Similar to the results under white light, *phyB-9* cotyledons showed enhanced chlorosis compared to the wild type following combined warm temperature and MeJA treatment (Supplementary Fig. 3e, f). Together, these results indicate that phyB suppresses, whereas COI1 promotes, the JA- and warm temperature-mediated inhibition of cotyledon chloroplast development.

phyB physically interacts with JAZ1 and JAZ3

JAZ proteins serve as central repressors in the JA signaling pathway (Hu et al., 2023). In our previous work, we generated green fluorescent protein (GFP)-fused transgenic lines for several *JAZ* genes and demonstrated that JAZ3 regulates seedling morphogenesis in response to light and warm temperature (Huai et al., 2024). Based on this, we hypothesized that phyB might functionally interact with JAZ proteins. To test this, we created homozygous *35S:JAZ1-GFP phyB-9* and *35S:JAZ3-GFP phyB-9* lines through genetic crossing. Under the 28℃+MeJA condition, both *35S:JAZ1-GFP phyB-9* and *35S:JAZ3-GFP phyB-9* seedlings largely retained green cotyledons and displayed chlorophyll contents comparable to their respective overexpression lines (Supplementary Fig. 4). This suggests that JAZ1 and JAZ3 act largely downstream of phyB in regulating cotyledon chlorophyll accumulation.

We next conducted a series of experiments to investigate their potential interaction. First, a yeast two-hybrid assay showed that while full-length (FL) phyB (fused with the GAL4 activation domain, GAD) interacted only weakly with JAZ1 (fused of the GAL4 DNA-binding domain, GBD), the C-terminal fragments of phyB (C651 or C451) strongly interacted with both JAZ1-GBD and JAZ3-GBD (Fig. 3a). Second, a luciferase complementation imaging (LCI) assay in *Nicotiana benthamiana* leaves revealed that co-expression of either JAZ1-nLUC (N-terminal half of firefly luciferase) or JAZ3-nLUC with phyB-cLUC (C-terminal fragment of luciferase) produced strong luminescence signals compared to controls (Fig. 3b). Third, bimolecular

fluorescence complementation (BiFC) assays in Arabidopsis protoplasts showed that co-transformation of phyB-nYFP (N-terminus of yellow fluorescent protein) and JAZ1-cYFP (C-terminal half of YFP) or JAZ3-YFP reconstituted YFP fluorescence specifically to the nucleus (Fig. 3c). Furthermore, we performed co-immunoprecipitation (Co-IP) experiments using *35S:JAZ1-GFP* and *35S:JAZ3-GFP* transgenic lines, with or without *35S:Myc-phyB*. When plants were grown at 22°C, Myc-phyB was co-precipitated with anti-GFP beads in samples from *35S:JAZ1-GFP 35S:Myc-phyB* and *35S:JAZ3-GFP 35S:Myc-phyB* seedlings. This interaction was markedly reduced after transferring the plants to 28°C for 3 h (Fig. 3d, e), indicating that warm temperature attenuates the phyB-JAZ association. Finally, an *in vitro* pull-down assay confirmed that Glutathione S-transferase fused to phyB (GST-phyB-C1), but not GST alone, could pull down His-tagged JAZ1 and His-JAZ3 (Fig. 3f, g). Together, these results demonstrate that phyB directly interacts with JAZ1 and JAZ3, and that warm temperature can weaken this interaction.

phyB regulates the protein stability of JAZ1 and JAZ3

The interaction between phyB and JAZ1/JAZ3 led us to investigate how phyB influences the properties of these JAZ proteins. Since JA promotes the ubiquitination and subsequent 26S proteasome-dependent degradation of JAZ proteins (Thines et al., 2007), we examined whether phyB affects the ubiquitination of JAZ1/JAZ3 under exogenous MeJA treatment. To capture transient ubiquitination signals, the proteasome inhibitor Bortezomib (Btz) was included to allow accumulation of poly-ubiquitinated proteins. Six-day-old *35S:JAZ1-GFP* and *35S:JAZ1-GFP phyB-9* plants were grown at 22°C or 28°C and treated with 100 μM MeJA for an additional 3 h at the respective temperature. After MeJA treatment and immunoprecipitation with anti-GFP beads, ubiquitinated JAZ1 levels were strongly increased in *35S:JAZ1-GFP* samples at both temperatures, as expected (Fig. 4a, b). Notably, ubiquitinated JAZ1 levels were further elevated in *35S:JAZ1-GFP phyB-9* plants compared to *35S:JAZ1-GFP* at 22°C, but this difference was not apparent at 28°C (Fig. 4a, b). This suggests that phyB inhibits JAZ1 ubiquitination in a temperature-dependent manner. Similar results were observed for JAZ3 ubiquitination (Supplementary Fig. 5a, b).

We next examined how phyB regulates JAZ1/JAZ3 degradation. First, the addition of MG132 (a 26S proteasome inhibitor) blocked MeJA-induced degradation of JAZ1 and JAZ3 in *35S:JAZ1-GFP* and *35S:JAZ3-GFP* plants, respectively, at 22℃. Moreover, JAZ1-GFP and JAZ3-GFP protein levels were lower in the *phyB-9* mutant background (*35S:JAZ1-GFP phyB-9* and *35S:JAZ3-GFP phyB-9*, respectively) (Fig. 4c; Supplementary Fig. 5c). Second, time-course degradation experiments showed that JAZ1-GFP and JAZ3-GFP levels gradually decreased in *35S:JAZ1-GFP* and *35S:JAZ3-GFP* seedlings, respectively, upon MeJA treatment at 22℃. This degradation was accelerated in the corresponding *phyB-9* mutant lines (Fig. 4d; Supplementary Fig. 5d). When the same treatments were applied at 28℃, the differences in MeJA-triggered degradation of JAZ1 between *35S:JAZ1-GFP* and *35S:JAZ1-GFP phyB-9*, and of JAZ3 between *35S:JAZ3-GFP* and *35S:JAZ3-GFP phyB-9*, were less pronounced than those observed at 22℃ (Fig. 4e, f; Supplementary Fig. 5e, f). Consistently, JAZ1-GFP and JAZ3-GFP protein levels were substantially reduced in the *phyB-9* background under 22℃, 22℃+MeJA, and 28℃ conditions, but the reduction was less marked under 28℃+MeJA (Supplementary Fig. 6a, b). Furthermore, we purified recombinant His-JAZ1 and His-JAZ3 proteins and performed an *in vitro* cell-free degradation assay. A time-dependent decrease in JAZ1 and JAZ3 was observed in Col-0 extracts, and this reduction was significantly delayed in extracts from *35S:Myc-phyB* plants in the presence of ATP (Supplementary Fig. 6c, d). Together, these results indicate that phyB suppresses JA-induced degradation of JAZ1/JAZ3 at normal temperature, but this suppressive effect is attenuated under warm temperature conditions.

HY5 and MYC2/MYC3/MYC4 transcription factors oppositely regulate JA/warm temperature-mediated responses

We hypothesized that certain downstream transcription factors in the warm temperature and JA signaling pathways might be involved in regulating cotyledon and chloroplast development. HY5 and PIFs are major components of the phyB pathway (Toledo-Ortiz et al., 2014; Liu et al., 2017; Xiao et al., 2022), while MYC transcription factors play central roles in JA-dependent seedling

morphogenesis (Ortigosa et al., 2020; Song et al., 2022). We performed phenotypic analyses and found that no discernible morphological differences were observed between these mutants and the wild type under 22℃, 22℃+MeJA, or 28℃ alone (Supplementary Fig. 7; Supplementary Fig. 8). Strikingly, after 28℃+MeJA treatment, while the three *pif* mutants (*pif1 pif3*, *pif4-1*, *pifq*) showed mild yellowing and marginally reduced chlorophyll levels similar to Col-0, the *hy5-215* mutant displayed severe cotyledon chlorosis with a decrease in chlorophyll content (Fig. 5a, b; Supplementary Fig. 7). Conversely, the *myc2-2* and *myc2/3/4* mutants retained higher chlorophyll contents than Col-0, while the *35S:MYC2-Myc* seedlings exhibited a wild-type-like phenotype (Fig. 5a, b; Supplementary Fig. 8). These results suggest that HY5 and MYC2/MYC3/MYC4 regulate cotyledon development in response to combined JA and warm temperature.

We next performed detailed characterization of the *hy5-215* and *myc2/3/4* mutants. Under the 28℃+MeJA condition, *myc2/3/4* mutants maintained significantly higher PSII photochemical efficiency, whereas *hy5-215* mutants showed lower Fv/Fm compared to Col-0 (Fig. 5c, d). Consistent with this, *myc2/3/4* mutants preserved intact thylakoid architecture with well-stacked grana and continuous stromal lamellae, and exhibited a greater number of chloroplasts, larger chloroplast area, and stronger chlorophyll autofluorescence than Col-0 (Fig. 5e-i; Supplementary Fig. 9a). In contrast, *hy5-215* displayed hallmark features of chloroplast degeneration (Fig. 5e-i; Supplementary Fig. 9a). Furthermore, quantification of chloroplast distribution and ultrastructural integrity across mesophyll cells indicated chloroplast defects in approximately 26% of Col-0 cells, 12% of *myc2/3/4* cells, and 81% of *hy5-215* cells (Supplementary Fig. 9b, c).

Immunoblot analyses were performed to examine chloroplast protein homeostasis upon 28℃+MeJA treatment. Levels of Rubisco large and small subunits (RbcL/RbcS), light-harvesting complex II chlorophyll a/b-binding protein 3 (Lhcb3), and D1 (the core subunit of photosystem II) were elevated in *myc2/3/4* but decreased in *hy5-215* compared with Col-0. In contrast, the stress-responsive chaperon HSP70 was markedly reduced in *myc2/3/4* but induced in *hy5-215* (Supplementary Fig. 9d). Moreover, under prolonged warm temperature and MeJA treatment, HY5 protein levels declined, whereas MYC2 accumulated markedly (Supplementary Fig. 9e). Together,

these results demonstrate that HY5 and these MYCs oppositely regulate JA and warm temperature-mediated chloroplast development in the cotyledons.

Transcriptomic analysis of genes regulated by JA and warm temperature

To elucidate the molecular basis of JA- and warm temperature-mediated inhibition of chloroplast development, we harvested cotyledons from Col-0 seedlings grown under four conditions and performed RNA-seq analysis. Transcriptome analysis revealed 1,446, 1,958, and 2,576 differentially expressed genes (DEGs; fold-change ≥2, false discovery rate (FDR) < 0.05) under the 22℃+MeJA, 28℃, or 28℃+MeJA conditions, respectively, compared with the 22℃ control; 365 DEGs were common to all three treatments (Supplementary Fig. 10a, Supplementary Data 1). Gene ontology (GO) and biological process (BP) enrichment analyses indicated that 22℃+MeJA primarily regulated genes associated with environmental stress and JA signaling (Supplementary Fig. 10b). Treatment with 28℃ alone affected genes related to abiotic stress and abscisic acid (ABA) signaling (Supplementary Fig. 10c), whereas the 28℃+MeJA combination altered genes involved in the biological processes of defense response and responses to salt stress and hypoxia (Supplementary Fig. 10d). Notably, 811 genes were specifically regulated under 28℃+MeJA; among these, 469 up-regulated genes were enriched in biosynthesis of secondary metabolites and immune response, while 342 down-regulated genes were associated with cellular function, growth, and developmental regulatory processes (Supplementary Fig. 10e, f, Supplementary Data 2). Venn analysis further confirmed that 28℃+MeJA induced a greater number of DEGs than 22℃+MeJA (Supplementary Fig. 10g, Supplementary Data 3). Specifically, 22℃+MeJA regulated genes related to abiotic stress and JA response (Supplementary Fig. 10h), whereas 28℃+MeJA shifted the profile toward cellular response to hypoxia, water deprivation, ABA, and heat (Supplementary Fig. 10i). Together, these results suggest that warm temperature and JA signal activate stress responses but suppress growth processes, which underlie the cotyledon chlorosis phenotype.

Transcriptomic analysis of genes regulated by HY5 and MYC2/MYC3/MYC4

To identify genes specifically regulated by the HY5 and MYC transcription factors, we compared transcriptomic profiles of the *hy5-215* and *myc2/3/4* mutants with Col-0 under the 28℃+MeJA condition. Compared to Col-0, the *hy5-215* mutant showed 1,691 DEGs, with a roughly equal distribution for up- and down-regulated genes (Fig. 6a, b, Supplementary Data 4). In contrast, the *myc2/3/4* triple mutants displayed 1,828 DEGs, of which 1,434 were down-regulated (Fig. 6c, d, Supplementary Data 5), suggesting that these MYC transcription factors function primarily as transcriptional activators in this context. GO annotation revealed that HY5 promotes chloroplast development by up-regulating genes involved in photosynthesis light harvesting, delaying leaf yellowing and promoting cotyledon development (Rashotte et al., 2006; Cheng et al., 2008; Kim et al., 2016). Conversely, MYC2/3/4 activated genes associated with abiotic and biotic responses, JA and ABA signaling, and particularly those involved in senescence and chlorophyll degradation (Fig. 6f). Expression patterns of 6 representative genes were validated by RT-qPCR (Supplementary Fig. 11). Additionally, HY5 predominantly repressed biological processes related to abiotic stress and ABA response (Supplementary Fig. 12a), whereas MYC2/3/4 negatively regulated pathways such as “regulation of DNA-templated transcription” and “auxin signaling pathway” (Supplementary Fig. 12b).

In addition to genes uniquely regulated by HY5 or MYCs, we also identified shared targets by both transcription factors. Among these, 126 genes were down-regulated in *myc2/3/4* mutants but upregulated in *hy5-215* mutants, whereas 38 genes showed the opposite patterns. Furthermore, 43 genes were co-upregulated and 340 genes were co-downregulated in both mutants (Supplementary Fig.12c; Supplementary Data 6). Given the contrasting yellowing phenotypes of *myc2/3/4* and *hy5-215* mutants, we focused on the 126-gene cluster. These genes were predominantly associated with stress responses, with a smaller subset linked to leaf senescence and chlorophyll catabolism (Supplementary Fig. 12d, e). RT-qPCR confirmed that three representative genes, *SAG21*, *MES16,* and *RAP2.6*, were consistently down-regulated in *myc2/3/4* but up-regulated in *hy5-215* under 28℃+MeJA treatment (Supplementary Fig. 12f). Collectively, these results establish HY5 and

MYCs as central hubs that integrate warm temperature and JA signaling during cotyledon development, with HY5 promoting growth- and chloroplast-related genes, and MYCs activating stress- and senescence-related pathways.

Genome-wide identification of direct targets of HY5 and MYC2

Given that HY5 and MYC2 are transcription factors, we performed DNA affinity purification sequencing (DAP-seq) to identify their genome-wide binding sites. A total of 17,633 HY5-binding peaks were identified (Supplementary Data 7), with 3,770 peaks consistently detected across two technical replicates (Supplementary Fig. 13a). Functional distribution analysis showed that 95.87% of peaks resided in gene-associated regions, of which >80% localized to promoters, while only 4.13% were in intergenic regions (Supplementary Fig. 13b). HY5 exhibited strong binding enrichment near the transcription start sites (TSS) of target genes (Fig. 7a). For MYC2, 3,566 common binding peaks were identified (Supplementary Fig. 13c, and Supplementary Data 8). Spatial distribution analysis revealed strong MYC2 binding near TSS (Fig. 7b), predominantly within promoter regions (Supplementary Fig. 13d). *De novo* motif analysis identified a highly enriched 10-bp conserved sequence ("HCACGTGGCA"; E-value = 1.0e-393) for HY5 (Fig. 7c). Similarly, a significantly enriched motif (Motif 9) containing a 13-bp conserved sequence "ACACGTGHYWWAW" (E-value = 1.2e-25) was identified for MYC2 (Fig. 7d). The core motif "CACGTG" corresponds to the canonical G-box recognized by both HY5 and MYC2, confirming the reliability of the data.

To identify direct targets of HY5 and MYC2, we integrated DAP-seq and RNA-seq data. Among the putative HY5 target genes from DAP-seq data, 660 genes (262 up-regulated and 398 down-regulated) were differentially expressed in the *hy5-215* mutant under 28℃+MeJA treatment (Supplementary Fig. 13e, Supplementary Data 9). These genes were primarily associated with organ development, hormone-mediated signaling pathway and DNA templated transcription (Supplementary Fig. 13f). Strikingly, 8 genes directly associated with cotyledon development were identified, and heatmap analysis showed that *WAVY GROWTH 2* (*WAG2*) and

CYTOKININ RESPONSE FACTOR (*CRF3*) were significantly enriched among HY5 targets (Fig. 7e). In addition, 8 representative genes responsive to stress and hormone signaling were selected for visualization (Fig. 7f). Similarly, by comparing DEGs in *myc2/3/4* mutants with MYC2 binding sites, we identified 202 potential direct target of MYC2 (33 up-regulated and 169 down-regulated) (Supplementary Fig. 13g, Supplementary Data 10). GO analysis revealed that many stress-responsive pathways ranked among the top ten enriched terms (Supplementary Fig. 13h), consistent with the role of MYC2 in JA-mediated cotyledon chlorosis. Heatmap analysis revealed that 9 genes involved in leaf morphogenesis and 5 JA-responsive genes were enriched among MYC2 targets (Fig. 7g). Genome-wide distribution analysis detected MYC2 occupancy peaks in the promoter regions of *Related to AP2 2.6* (*RAP2.6*) (Supplementary Fig. 13i). Together, these analyses demonstrate that HY5 and MYC2 target a broad set of downstream genes related to cotyledon development and JA response.

HY5 and MYC2 directly activate the expression of chloroplast development-related genes

We then selected several representative downstream target genes to validate the DAP-seq findings. Golden-Like 1 (GLK1) is a well-known transcription factor that controls chloroplast development (Li et al., 2025). HY5 fused to the activation domain (AD-HY5) and drove the expression of the *LacZ* reporter under the control of the *GLK1*, *GLK2*, *WAG2*, *COLD-REGULATED 15B* (*COR15B*), *9-cis-epoxycarotenoid dioxygenase 3* (*NCED3*), or *LOW-TEMPERATURE-INDUCED 65* (*LTI65*) promoter in yeast cells (Supplementary Fig. 14a). Similarly, AD-MYC2 directly bound to the promoter of *NON-YELLOW COLORING 1* (*NYC1*), *SUPPRESSOR OF OVEREXPRESSION OF CONSTANS 1* (*SOC1*), *MYB47*, *Acyl-CoA-Binding Protein 3* (*ACBP3*), *HSP101* or *RAP2.6* and activated reporter expression (Supplementary Fig. 14b). Promoter analysis identified the presence of multiple motifs in the *GLK1* promoter (Fig. 8a). To examine whether HY5 binds the promoter *in vivo*, we performed chromatin immunoprecipitation followed by quantitative PCR (ChIP-qPCR) using a *35S:HY5-GFP* transgenic line. The result showed that HY5 directly associated with the *GLK1* promoter at the 22℃ or 28℃ conditions. Notably, this binding was attenuated under

28℃+MeJA treatment (Fig. 8b). In contrast to HY5, MYC2 bound specifically to the *RAP2.6* promoter only under the 28℃+MeJA condition, with no significant binding detected at 22℃ or 28℃ alone (Fig. 8c, d). These results demonstrate that HY5 preferentially binds its target genes under normal growth condition, whereas MYC2 binding occurs predominantly under combined warm temperature and JA treatment.

To assess the transcriptional activation capacity of HY5 and MYC2 on their target genes, we conducted a transient expression assay in Arabidopsis protoplasts. Effector constructs (*35S:HY5-HA*, *35S:MYC2-HA,* or an empty vector control) were co-expressed with reporter constructs in which the *LUC* gene was driven by various promoters. HY5-HA significantly activated *LUC* expression under the control of *GLK1*, *WAG2*, *COR15B*, or *LTI78* promoter compared with the vector control (Fig. 8e, f). MYC2-HA strongly activated *LUC* expression driven by the *NYC1*, *SAG20*, *RAP2.6*, or *SAG21* promoter (Fig. 8g, h). Further analysis revealed that HY5 transcriptional activity was reduced in the *phyB* mutant background, whereas MYC2 activity remained independent of COI1 (Supplementary Fig. 15a, b). We next examined whether warm temperature and JA influence the function of HY5 and MYC2. Protoplasts expressing the effector-reporter constructs were treated with or without 10 μM MeJA for 3 h at 22℃ or transferred to 28℃ for the same period before luciferase measurement. HY5-mediated activation of *WAG2* was consistently observed under 28℃ or MeJA alone and was further enhanced under 28℃+MeJA (Supplementary Fig. 15c). MYC2-driven activation of *RAP2.6* was markedly enhanced under 28℃ or 28℃+MeJA conditions (Supplementary Fig. 15d). Together, these findings demonstrate that HY5 and MYC2 function as key transcription factors integrating warm temperature and JA signaling during chloroplast development.

Discussion

The integration of internal hormonal cues and external temperature signal is crucial for plant growth, development, and ecological adaptation. Our study delineates a hierarchical signaling network in which phyB integrates warm temperature perception and JA signaling through JAZ

proteins, HY5, and MYC transcription factors. We demonstrate that phyB and COI1 play opposing roles in this developmental outcome by modulating JAZ protein stability. The antagonistic interplay between HY5 and MYC2 translates the JA and warm-temperature signals into transcriptional programs that determine chloroplast fate during cotyledon development (Fig. 9).

Synergistic effects of JA and warm temperature on cotyledon and chloroplast development

While both JA and warm temperature independently promote chlorophyll degradation and leaf senescence (Zhu et al., 2015; Kim et al., 2020), their combined effect, particularly during early seedling development, has remains unexplored. Focusing on the cotyledon stage, we demonstrate that simultaneous exposure to warm temperature and MeJA induces synergistic deterioration of cotyledons. These observation align with previous reports that JA accelerates senescence under stress and that high temperature destabilizes photosynthetic complexes (Zhu et al., 2015; Kim et al., 2020). However, the synergistic interaction betwen temperature and JA revealed here highlights a previously underappreciated layer. Warm temperature alone mildly reduced chlorophyll content but increased cotyledon area (Fig. 1b), likely reflecting thermomorphogenesis-driven cell expansion (Quint et al., 2016). In contrast, the combination of JA and warm temperature shifted the balance toward catabolic processes, as indicated by reduced chloroplast number, disrupted thylakoid membranes (Fig. 1f-k), and down-regulation of chloroplast development-related genes (Supplementary Fig. 11a-c). Concurrent up-regulation of *RAP2.6* and *SAG21* supports a model in which warm temperature amplifies JA-induced cotyledon chlorosis (Supplementary Fig. 12f). Similar synergistic effects have been reported for ABA and JA in drought responses, indicating that hormone-environment interplay often drives hyperactivated stress responses (de Ollas and Dodd, 2016). RNA-seq analysis further revealed that JA and warm temperature synergistically activate stress-related pathways while repressing growth-related and cell cycle genes, illustrating a profound stress response consistent with the “defense-growth trade-off”paradigm. Our results underscore the convergence on stress-response pathways and

suppression of growth, representing an adaptive strategy that reallocates resources from development to stress mitigation.

phyB integrates thermo-JA crosstalk by regulating JAZ stability

Previous results have demonstrated that inactivation of phyB, through a low red-to-far-red light ratio or by mutation, reduces JA production and down-regulation of JA-dependent gene expression (Moreno et al., 2009). Field evidence also suggests that shading or high planting density attenuates JA-mediated defense responses (Suzuki et al., 2011; Agrawal et al., 2012). However, the mechanisms linking between phyB and JA signaling remain incompletely understood and likely operate at multiple regulatory levels. Here, we show that phyB and COI1 antagonistically regulate chloroplast development in seedlings (Fig. 2; Supplementary Fig. 3). Notably, this regulatory pattern resembles the recent described role of NPR1 in degrading PIF4 to coordinate light and immune responses (Zhou et al., 2024), pointing to an evolutionarily conserved "hormone receptor-environmental sensor" framework that facilitates environmental adaptation.

The stability and spatiotemporal regulation of JAZ proteins are critical for fine-tuning JA signaling outputs, and their degradation or stabilization is governed by diverse post-translational mechanisms (Xu et al., 2024b). While the canonical SCF^{COI1} E3 ligase complex mediates JA-dependent ubiquitination of specific JAZ members (Xu et al., 2002; Yan et al., 2013), emerging evidence highlights alternative regulators; e.g. SKIP31 targets JAZ6/JAZ11 during seed maturation (Varshney et al., 2023), and PUB22 ubiquitinates JAZ4 to enhance herbivore resistance (Wu et al., 2024). In this study, we identify phyB as an important stabilizer of JAZ proteins, as evidenced by accelerated JA-induced JAZ1/JAZ3 degradation and increased polyubiquitination levels in the *phyB-9* mutants (Fig. 4; Supplementary Fig. 5). phyB may confer stabilization via two non-exclusive pathways: direct JAZ binding and indirect suppression of COI1 E3 ligase activity. Importantly, this stabilization is temperature-dependent; the interaction between phyB and JAZ is attenuated under warm temperature (Fig. 3d, e), likely due to the reduction of nuclear phyB-Pfr. This function is distinct from the classical role of phyB in light signaling and underscores its

function as a thermosensory integrator that links temperature cues to JA-responsive proteostasis through dynamic control of JAZ protein turnover.

HY5 and MYC2 antagonistically regulate gene expression and responses

phyB orchestrates cotyledon chlorosis through multiple pathways, primarily via PIFs (e.g., PIF4 and PIF5), which regulate chlorophyll degradation (Sakuraba et al., 2014; Zhang et al., 2015). However, our findings indicate that HY5 acts as the dominant effector downstream of phyB during JA/warm temperature-mediated chloroplast development. HY5 potentially mediates retrograde signaling from plastids to the nucleus, thereby balancing stress responses with organelle homeostasis (Li et al., 2022b). This aligns with the dual role of HY5 in photomorphogenesis and chloroplast maintenance as it directly activates chlorophyll biosynthesis genes (e.g., *CHLH*, *PORC*) and stabilizes chloroplast development (Toledo-Ortiz et al., 2014; Zhang et al., 2024; Li et al., 2025). Transcriptomic profiling reveals that HY5 serves as a potent repressor of stress-accelerated senescence pathways. By suppressing key senescence-promoting genes and stress-responsive factors (Supplementary Fig. 12), HY5 actively prevents premature cotyledon chlorosis. Mechanistically, HY5 directly binds to the G-box cis-element within the promoters of pivotal development- and stress-related genes, thereby activating their transcription (Fig. 7c, e, f; Fig. 8f; Supplementary Fig. 14a). Notably, HY5 also integrates light and stress signals to modulate autophagy, enhancing the expression of *ATGs* genes to sustain chloroplast function under nutrient deprivation (Yang et al., 2020). Hence, beyond its established functions in photomorphogenesis, HY5 emerges as a crucial integrator of environmental cues.

Emerging evidence suggests that JA as a dual-function hormone that not only promotes senescence but also actively suppresses leaf growth through evolutionarily conserved mechanisms (He et al., 2002; Noir et al., 2013; Attaran et al., 2014). Our study identifies MYC proteins as key mediators of COI1-dependent JA signaling, which orchestrates chloroplast homeostasis in response to JA and warm temperature. Transcriptomic analysis indicates that MYC proteins predominantly function as transcriptional activators of JA-responsive, stress-related, and

senescence-associated genes, while exerting only marginal repressive effects on photosynthesis-related genes (Fig. 6f and Supplementary Fig. 11). Our results demonstrate that warm temperature and JA significantly enhance the DNA-binding affinity and transcriptional activation of MYC2 (Fig. 8d; Supplementary Fig. 15d). Notably, chloroplasts in the *myc2/3/4* mutants exhibit intact ultrastructure, featuring tightly stacked thylakoid membranes, which suggests that MYC proteins may directly regulate thylakoid biogenesis. This function contrasts with the GLK-MYB regulatory axis involved in chloroplast development (Frangedakis et al., 2024). Our finding indicates that MYCs play a role in regulating thylakoid membrane biogenesis to maintain chloroplast homeostasis, revealing a previously unrecognized function for MYC2 in this process. We thus discover a complex antagonistic relationship between HY5 and MYC2 in the regulation of chloroplast development.

Methods

Plant materials and growth conditions

The Arabidopsis wild type is of the Columbia (Col-0) ecotype. The *phyB-9* (Reed et al., 1993), *hy5-215* (Oyama et al., 1997), *pif1 pif3* (Li et al., 2023), *pif4-1* (Huai et al., 2018), *pifq* (Zhang et al., 2014), *coi1-8* (Xu et al., 2002b), *myc2-2* (SALK_083483), *my2/3/4* (Fernández-Calvo et al., 2011), *35S:COI1-GFP*, *35S:JAZ1-GFP*, *35S:JAZ3-GFP* (Huai et al., 2024), *35S:MYC2-Myc* (An et al., 2017), *35S:Myc-phyB* (Liu et al., 2021), and *35S:HY5-GFP* (Jing et al., 2020) lines were reported previously. All mutants were validated using PCR genotyping and sequencing. The double mutant/transgenic lines were generated by genetic crosses and verified via phenotypic assessment, antibiotic selection, PCR genotyping and/or sequencing. The seeds were surface-sterilized and sown on Murashige and Skoog (MS) medium with different concentrations of MeJA (392707, Sigma-Aldrich) containing 1% sucrose and 0.6% agar. The seeds were subsequently stored in darkness at 4℃ for 3 days, and then exposed to continuous white light (40 μmol m^{-2} s^{-1}) or red light (40 μmol m^{-2} s^{-1}) at either 22℃ or 28℃ for 6 days using light-emitting diodes. The

adult plants were grown in proximity in soil within a growth chamber, under long-day conditions (16 hours light / 8 hours dark), with 60-70% humidity at 22 ± 2℃. Phenotypes were documented using a stereomicroscope (Nikon, http://www.nikon.com). Cotyledon area was measured for at least 20 individual seedlings using ImageJ software (http://rsbweb.nih.gov/ij/).

Chlorophyll measurement

Chlorophyll measurement was conducted following the previously described method (Zhang et al., 2017). Briefly, twenty seedlings were weighed and subsequently extracted with 80% acetone in the dark for a duration of 6 hours. The absorbance was measured at 663 nm and 647 nm, and total chlorophyll contents was calculated as ($7.15\times A_{663} +18.71\times A_{647}$) and expressed as mg per gram fresh weight (mg/g FW).

Chloroplast morphology analysis

For confocal laser scanning microscopy, cotyledons of 6-day-old seedlings were excised and mounted on glass slides. Microscopic imaging was performed using an Olympus FV1000MPE multiphoton fluorescence lifetime system equipped with a 63× water-immersion objective. Fluorescence detection parameters were set as excitation wavelength (488 nm) and emission spectral collection (490-585 nm). Images were acquired using a Z-stack scanning mode (0.5 μm step size) and processed via multi-focal plane image fusion. Subsequent image analysis and data export were conducted using FV10-ASW software (v4.2). For quantitative analysis, ImageJ software was employed to evaluate chloroplast density (number per cell area), mean chloroplast area, and mean chlorophyll autofluorescence intensity normalized to the corresponding chloroplast area.

Chlorophyll fluorescence imaging

To assess photosynthetic efficiency, seedlings were dark-adapted for 30-minute prior to measurements. Chlorophyll fluorescence imaging system (Imaging-PAM, WALZ) was used to determine the maximum quantum yield of photosystem II (ΦPSII) and effective quantum yield of PSII (Fv/Fm), and qP (coefficient of photochemical quenching). The ETR and redox state of the

Q_A electron acceptor of PSII (1-qP) were analyzed as previously described (Liu et al., 2024). During the experiment, a continuous actinic light (80 μmol m^{-2} s^{-1}) was applied as the background illumination. To determine the maximum fluorescence yield under light-adapted conditions (Fm'), the system delivered saturating pulse light (2800 μmol m^{-2} s^{-1}) at 20-second intervals. All fluorescence parameters were acquired and processed using ImagingWin software.

Transmission electron microscopy

The samples were fixed overnight at 4℃ in a solution containing 3% (w/v) glutaraldehyde in 0.1 M Phosphate-Buffered Saline (PBS), pH 7.2. After fixation, they were washed three times (30 min each) with 0.1 M PBS buffer and post-fixed with 2% osmium tetroxide (OsO_4) in the same buffer at 4℃ for 3 h. For dehydration, the samples were treated with a graded ethanol series (50%, 70%, and 90% ethanol, 30 min each) This was followed by two changes of anhydrous ethanol (30 min each, RT). Next, the samples were transitioned into acetone (two changes, 30 min each) and infiltrated with Quetol-651 epoxy resin (Nisshin EM, Tokyo, Japan) using a 50:50 acetone: resin mixture (3 h), followed by pure resin (3 h). Polymerization was carried out at 60℃ for 24 h. Ultrathin sections (80 nm thick) were cut using an ultramicrotome (Ultracut UCT, Leica) equipped with a diamond knife and mounted onto copper grids. The sections were stained with 1% uranyl acetate (15 min, RT), rinsed with distilled water, and then counterstained with lead citrate (3 min, RT) (Sigma-Aldrich). TEM imaging was performed using a JEOL JEM-1230 microscope (80 kV acceleration voltage). Digital images (3296× 2472 pixels) were acquired with a CCD camera (EM-14830RUBY2, JEOL). Microscopy observations were conducted by Tokai Electron Microscopy (Nagoya). Ultrastructural analysis was performed on transmission electron micrographs to quantitatively assess chloroplast morphology. To ensure statistical robustness, at least 50 grana were randomly selected and analyzed per condition from a minimum of 10 chloroplasts. All micrographs were captured at a standardized magnification and calibrated using an internal scale bar. The thylakoid stacking number per granum quantified on a per-chloroplast-profile basis using ImageJ software.

Plasmid construction

The coding sequences or fragments of *phyB*, *JAZ1*, *JAZ3*, *HY5*, and *MYC2* were amplified from Col-0 genomic DNA or cDNA using KOD DNA Polymerase (TOYOBO). The resulting DNAs were cloned into the pEASY-Blunt Simple vector (CB111, TransGen) and verified by sequencing. Various plasmids and vectors were digested with the appropriate restriction enzymes, ligated and transformation into *E. coli* Trans-T1 (TransGen) chemically competent cells.

For yeast one-hybrid assay, promoter fragments of *GLK1*, *GLK2*, *WAG2*, *COR15B*, *LTI65*, *NCED3*, *NYC1*, *SOC1*, *MYB47*, *HSP101*, *ACBP3*, and *RAP2.6* were amplified from Col-0 genomic DNA and inserted into the EcoR1-SalI sites of pLacZi-2μ (Lin et al., 2007) using a Seamless Assembly Cloning kit (C5891-100, CloneSmarter), to generate *pGLK1:LacZ*, *pGLK2:LacZ*, *pWAG2:LacZ*, *pCOR15B:LacZ*, *pLTI65:LacZ*, *pNCED3:LacZ*, *pNYC1:LacZ*, *pSOC1:LacZ*, *pMYB47:LacZ*, *pHSP101:LacZ*, *pACBP3:LacZ*, and *pRAP2.6:LacZ*, respectively. To obtain AD-HY5, AD-MYC2, their coding sequences were amplified and cloned into the EcoRI-XhoI sites of pB42AD/pJG4-5 (hyykb101, Clontech).

For yeast two-hybrid assay, the full-length JAZ1/JAZ3 sequences were released from their respective pEASY plasmids using EcoRI and SalI, and inserted into the EcoRI-SalI sites of the pGBKT7 vector (PT3248-5, Clontech) to generate JAZ1-GBD, and JAZ3-GBD, respectively. The phyB-GAD, phyB-C451-GAD, and phyB-C651-GAD plasmids were produced as previously described (Liu et al., 2021).

For transient LCI assay, the full-length coding sequences of JAZ1/JAZ3 were amplified and inserted into the KpnI-SalI sites of pCAMBIA1300-nLUC, generating JAZ1-nLUC and JAZ3-nLUC. The phyB-cLUC plasmid was described previously (Liu et al., 2021).

For recombinant protein expression, the full-length coding sequences of JAZ1/JAZ3 were amplified and inserted into the EcoRI-SalI sites of the pCold-His-TF (3365, Takara) by recombination, resulting in His-JAZ1 and His-JAZ3, respectively. The GST-phyB-C1 plasmid was described previously (Liu et al., 2021).

For BiFC assay, the full-length phyB and JAZ1/JAZ3 were inserted into pSAT4A-nYFP or pSAT4A-cYFP to generate phyB-nYFP, JAZ1-cYFP, and JAZ3-cYFP respectively.

For transient expression in Arabidopsis mesophyll protoplasts and the transient luciferase reporter assay, MYC2 and HY5 were inserted into the pUC18-3HA vector to produce pUC18-MYC2-HA and pUC18-HY5-HA, respectively. The promoters of *WAG2*, *GLK1*, *COR15B*, *LTI78*, *NYC1*, *SAG20*, *RAP2.6*, and *SAG21* were amplified and cloned into the pGreenII 0800-LUC vector to generate *pWAG2:LUC*, *pGLK1:LUC*, *pCOR15B:LUC*, *pLTI78:LUC*, *pNYC1:LUC*, *pSAG20:LUC*, *pRAP2.6:LUC* and *pSAG21:LUC*, respectively. All primers were listed in Supplementary Table 1.

RNA isolation and RT-qPCR

RNA isolation and RT-qPCR were conducted as described previously (Li et al., 2022c). Six-day-old seedlings were harvested and immediately frozen in liquid nitrogen. Total RNA was extracted using the SteadyPure Universal RNA Extraction Kit (Accurate Biotechnology), followed by treatment with RNase-free DNase I (Thermo Fisher Scientific). The first-strand cDNA was synthesized from 1 μg of total RNA using an oligo (dT) primer and reverse transcriptase (Invitrogen). Quantitative real-time PCR (qRT-PCR) was conducted using the cDNA samples and SYBR Green I Master (Takara) on a Light-Cycler 480 (Roche) in accordance with the manufacturer's instructions. Data analysis and calculation were performed using the $2^{-\Delta\Delta CT}$ method based on three independent biological samples. Expression levels were normalized using *UBQ1* as the internal control. The sequences of primers are provided in Supplementary Table 1.

Yeast one-hybrid assay

The yeast one-hybrid assay was performed as described previously (Liu et al., 2021). Various LacZ reporter plasmids were co-transformed with either AD-HY5 or AD-MYC2 into the yeast strain EGY48. The resulting transformants were grown on SD/-Ura-Trp dropout plates supplemented with X-gal (5-bromo-4-chloro-3-indolyl-β-D-galactopyranoside) for color development.

Yeast two-hybrid assay

The yeast two-hybrid assay was conducted as described previously (Li et al., 2022c). The GBD-fusion and GAD-fusion plasmids were co-transformed into the yeast strain Y2H Gold and subsequently selected on SD/-Leu-Trp (LW) dropout medium. Growth on SD/-Leu-Trp-His-Ade (LWHA) dropout medium indicated a positive protein-protein interaction.

LCI assay

The nLUC/cLUC-fusion constructs and empty plasmid were introduced into Agrobacterium strains GV3101 separately and subsequently resuspended in infiltration buffer [10 mM $MgCl_2$, 10 mM MES (pH 5.6), 200 μM acetosyringone] to a final OD_{600} of 1.0-1.5. Different nLUC/cLUC-fusion constructs were mixed with an equal volume of conjugative p19 plasmid suspension. The bacteria mixtures were incubated at 28℃ for 2-3 hours and then introduced into the young leaves of 5-week-old *N. benthamiana* plants grown in a growth chamber. Leaves were collected 2 days after the infiltration and sprayed with 2 μM D-luciferin (dissolved in 0.02% Triton X-100, v/v) for the detection of luciferase signals using a NightSHADE LB985 plant imaging system fitted with a CCD camera (Berthold Technologies). Experiments were performed at least three times with consistent results.

BiFC assay

The BiFC assays were performed as described (Li et al., 2022c). Plasmids expressing N- and C-terminal YFP fusion proteins were co-transfected into Arabidopsis protoplasts. The protoplasts were incubated in darkness for 12 to 16 hours. Yellow fluorescent protein (YFP) signals were observed using a confocal microscope (Zeiss LSM 980).

Pull-down assay

Recombinant His-JAZ1, His-JAZ3 and GST-phyB-C1 fusion proteins were expressed in *Escherichia coli* BL21 (DE3) strain and induced with isopropyl β-D-thiogalactopyranoside at 16℃. 5 μg of bait protein (GST-phyB-C451 or GST) and 5 μg of prey protein (His-JAZ1/His-JAZ3) were combined with 1 mL of binding buffer [50 mM Tris-HCl pH 7.5, 150 mM NaCl, 10% (w/v) glycerol and 0.5% (v/v) Triton X-100]. After mixing, 10 μL of Glutathione Sepharose 4B beads

(BE6948, EASYBIO) were added and the mixture was incubated at 4℃ for 1 hour. After washing the beads four times with washing buffer [50 mM Tris-HCl pH 7.5, 200 mM NaCl, and 1% (v/v) TritonX-100], the proteins were subsequently eluted using 2× SDS loading buffer at 95℃ for 8 min. The input and immunoprecipitation samples were separated by 8% SDS-PAGE gel, and proteins were detected by immunoblotting with anti-GST and anti-His antibodies.

Protoplasts transformation and transient luciferase reporter assay

Arabidopsis mesophyll protoplasts were isolated from 4-week-old Col-0 plants as described previously (Li et al., 2022c). Protoplasts were co-transformed with 5 μg of reporter plasmids and 5 μg of effector plasmids. After incubation in darkness for 16 hours, protoplasts were lysed, and the activities of LUC and REN were quantified using a Dual-Luciferase Reporter Assay System (E1910, Promega).

Protein immunoblotting

For immunoblotting of JAZ1/JAZ3-GFP and photosystem proteins, samples were homogenized in extraction buffer [50 mM Tris-HCl (pH 7.5), 10 mM $MgCl_2$, 150 mM NaCl, 1 mM EDTA, 10% (w/v) glycerol, 1% (v/v) Triton X-100, 10 mM dithiothreitol (DTT), 1 mM phenylmethylsulfonylfluoride (PMSF), 1× EDTA-free protease inhibitor cocktail (4693159001, Roche), 25 μM MG132 (474790, Sigma-Aldrich)]. For immunoblotting of HY5 and MYC2 proteins, total proteins were extracted with buffer [50 mM Tris-HCl (pH 7.5), 10 mM $MgCl_2$, 150 mM NaCl, 1 mM EDTA, 10% (w/v) glycerol, 0.1% (w/v) Tween 20, 20 mM DTT, 1 mM PMSF, 1× EDTA-free protease inhibitor cocktail, 50 μM MG132]. Protein concentration was determined with Bradford assay reagent (Bio-Rad). Equal amounts of total proteins per sample were boiled in 10× SDS loading buffer for 10 min and separated by 8% or 10% SDS-PAGE gels. After transfer to polyvinylidene fluoride (PVDF) membranes, proteins were immunoblotted with primary antibodies followed by horseradish peroxidase-conjugated secondary antibody (CW0102S, CWBIO, 1:10,000). Signals were detected using a Chemiluminescence Imaging System (Biostep).

Co-IP assay

Protein extracts were incubated with GFP-Nanoab-agarose (GNA-50-1000, Lablead) for 2 hours at 4℃. Beads were washed three times with extraction buffer. After centrifugation at 1,000 *g* at 4℃ for 3 min, the precipitated proteins were eluted in 2× SDS loading buffer at 95℃ for 10 min. Proteins were subsequently separated by 10% SDS-PAGE gel and detected by immunoblotting with anti-GFP and anti-Myc antibodies.

***In vivo* ubiquitination assay**

The conventional ubiquitination assay was performed as described (Fan et al., 2023). Briefly, six-day-old plants were treated with 100 μM MeJA and 50 μM Bortezomib (Btz) (S1013, Selleck) for 3 h and ground to a fine powder in liquid nitrogen. Total proteins were extracted with protein extraction buffer [50 mM Tris-HCl pH 7.5, 150 mM NaCl, 0.1% (v/v) NP-40, 1% (v/v) Triton X-100,1 mM PMSF, 1× complete protease inhibitor cocktail, 50 μM N-ethylmaleimide (CE5162, Coolaber), 50 μM MG132, 1× complete protease inhibitor cocktail]. The supernatants were centrifuged twice at 4℃, 13,000 *g* for 10 min. The resulting supernatants were incubated with pre-washed GFP-Nanoab-agarose for 3 h at 4℃, and washed three times with washing buffer [50 mM Tris-HCl pH 7.5, 300 mM NaCl, 0.1% (v/v) NP-40, 1% (v/v) Triton X-100]. After centrifugation at 1,000 *g*, 4℃ for 3 min, the precipitated proteins were eluted in 2× SDS loading buffer at 95℃ for 10 min. Proteins were then separated by 10% SDS-PAGE gel and detected by immunoblotting with anti-GFP antibody and anti-UBQ11 rabbit polyclonal antibody (AS08307A, Agrisera).

Cell-free degradation assay

Cell-free degradation assays were performed as previously described (Xu et al., 2016). Total proteins extracts were prepared from six-day-old seedlings using extraction buffer [25 mM Tris-HCl (pH 7.5), 10 mM NaCl, 10 mM $MgCl_2$, 5 mM PMSF, 5 mM DTT and 2 mM ATP]. The crude extract was then centrifuged at 13,000 *g* at 4℃ to remove debris, and the supernatants were adjusted to equal protein concentrations using the Bio-Rad assay. For purified JAZ1/JAZ3-His protein degradation, 20 μg recombinant JAZ1-His or JAZ3-His protein was incubated in 100 μL

extract at 22℃ for 15, 30 and 60 min, then the reactions were stopped and the JAZ proteins were analyzed by immunoblotting using anti-His antibody (HT501; TransGen).

RNA-seq analysis

Col-0, *myc2/3/4* and *hy5-215* seeds were sown on MS medium supplemented with or without MeJA and grown under continuous white light at 22℃ or 28℃ for 6 days. Cotyledons were excised and harvested subsequently. Total RNA was extracted using an RNAprep Pure Plant Kit (Tiangen). Contaminating DNA was removed by digestion with RNase-free DNaseI (Tiangen) in accordance with the manufacturer's instructions. Samples were submitted to Biomarker Biotechnology Corporation, Inc for sequencing. Three biological replicates were collected per genotype. Genes exhibiting a FC (Fold Change) ≥ 2 and FDR (False discovery rate) < 0.05 were identified as differentially expressed genes (DEGs). The GO enrichment analysis was performed utilizing the online tool (https://david.ncifcrf.gov/conversion.jsp). GO terms with FDR < 0.05 were considered significantly enriched. GO term enrichment diagrams were generated using the website (https://www.chiplot.online/#BioPlot).

DAP-seq sampling and data analysis

DAP-seq was performed as previously described (O'Malley et al., 2016). Genomic DNA (gDNA) was extracted from the cotyledons of 6-day-old Col-0 seedlings grown on MS medium with 25 μM MeJA under continuous white light at 28℃ and purified by Bluescape Biotech (Hebei) and SeqHealth Tech (Wuhan). The fragmented gDNA was then used to construct libraries with the NEXTFLEX Rapid DNA-Seq Kit (PerkinElmer). The coding sequence of MYC2 and HY5 were cloned into a pFN19K HaloTag T7 SP6 Flexi vector and expressed using the TNT SP6 Coupled Wheat Germ Extract System (Promega). The expressed protein was purified and captured using Magne HaloTag Beads (Promega). The MYC2 and HY5-bound beads were incubated with adapter-ligated gDNA libraries. Eluted DNA was sequenced on an Illumina NovaSeq 6000 platform with two technical replicates. A negative control (Input) was prepared by incubating the gDNA libraries with beads in the absence of protein. The DAP-seq reads were aligned to the reference genome (TAIR https://www.arabidopsis.org). Peaks were called using MACS2, and the

reproducibility of peaks between replicates was assessed using IDR ($p < 0.05$). MEME-CHIP was employed to identify conserved motifs within the peak regions, while Homer was used for peak annotation. GO enrichment analysis was performed utilizing the online tool (https://david.ncifcrf.gov/conversion.jsp). Target genes were defined as those with DAP-seq peaks located within 2 kb upstream of the ATG start codon.

ChIP-qPCR

ChIP assays were performed as described previously (Xu et al., 2024a). Briefly, plant tissues were crosslinked with 1% (v/v) formaldehyde under vacuum on ice for 15 min, and the reaction was quenched by adding 2 M glycine. Nuclei were isolated using lysis buffer (50 mM Tris-HCl, pH 8.0, 10 mM EDTA, 1% SDS, 0.1 mM PMSF, and 1× complete protease inhibitor cocktail). Chromatin was fragmented by sonication on ice to an average size of 250-500 bp. Immunoprecipitation was performed using anti-GFP antibody (D153-11, MBL) or anti-Myc antibody (M047-11, MBL), with goat anti-mouse IgG (HNM-25-1000, Lablead) as the negative control. Both input and ChIP samples were subjected to reverse crosslinking by incubation at 65℃ with Proteinase K overnight. DNA was subsequently purified by phenol extraction and recovered for analysis. qPCR was performed using Power SYBR Green Master Mix (Applied Biosystems) with gene-specific primers on immunoprecipitated DNA. Target gene promoter enrichment was presented as the percentage of input DNA, calculated by normalizing the immunoprecipitated DNA level against the input sample. *ACTIN7* was used as reference genes, and primer sequences were listed in Supplementary Table 1.

Antibody production and information

Anti-HY5 (Jing et al., 2020) was produced in-house. Other antibodies were purchased commercially: anti-Actin (CW0264M, CWBio), anti-GFP (HT801, TransGen), anti-Myc (HT101, TransGen), anti-His (HT501, TransGen), anti-GST (ab184804, Abcam), anti-MYC2 (A20774, ABclonal), anti-RbcL (AS03037, Agrisera), anti-RbcS (AS07259, Agrisera), anti-HSP70

(M20041F, Abmart), anti-Lhcb3 (AS01002, Agrisera), anti-D1(AS05084, Agrisera), and anti-UBQ11(AS08307A, Agrisera).

Statistical analysis

All data analysis and visualization were performed using GraphPad Prism (version 10.6) and Origin 2019b software. The values are presented as mean standard deviation (SD). Statistical significance was determined by two-way analysis of variance (ANOVA) followed Tukey's multiple comparison test. Differences were considered statistically significant at $p < 0.05$, and distinct letters are used in the figures to denote significant differences between groups.

Data availability

All data generated or analyzed in this study are available in the main text and the Supplementary Information. Sequence data from this article can be found in the GenBank/EMBL data libraries under the following accession numbers: *COI1* (AT2G39940), *phyB* (AT2G18790), *JAZ1* (AT1G19180), *JAZ3* (AT3G17860), *HY5* (AT5G11260), *MYC2* (AT1G32640), *MYC3* (AT5G46760), *MYC4* (AT4G17880), *MES16* (AT4G16690), *RAP2.6* (AT1G43160), *RAP2.6L* (AT5G13330), *SAG21* (AT4G02380), *SAG20* (AT3G10985), *SOC1* (AT2G45660), *NYC1* (AT4G13250), *SRG1* (AT1G17020), *WAG2* (AT3G14370), *CRF2* (AT4G23750), *NCED3* (AT3G14440), *COR15B* (AT2G42530), *MYB47* (AT1G18710), *ACBP3* (AT4G24230), *HSP101* (AT1G74310), *LTI65* (AT5G52300), *LTI78* (AT5G52310), *GLK1* (AT2G20570), *GLK2* (AT5G44190), *ACTIN7* (AT5G09810), and *UBQ1* (AT3G52590). All the unprocessed data, gels, and blots were provided in the Source Data file. Source data are provided with this paper.

References

Agrawal, A.A., Kearney, E.E., Hastings, A.P., & Ramsey, T.E. Attenuation of the jasmonate burst, plant defensive traits, and resistance to specialist monarch caterpillars on shaded common milkweed (*Asclepias syriaca*). *J. Chem. Ecol.* **38**, 893-901 (2012).

An, C., et al. Mediator subunit MED25 links the jasmonate receptor to transcriptionally active chromatin. *Proc. Natl. Acad. Sci. USA* **114**, E8930-E8939 (2017).

Attaran, E., et al. Temporal dynamics of growth and photosynthesis suppression in response to jasmonate signaling. *Plant Physiol.* **165**, 1302-1314 (2014).

Casal, J.J., & Balasubramanian, S. Thermomorphogenesis. *Annu. Rev. Plant Biol.* **70**, 321-346 (2019).

Chen, D., et al. Integration of light and temperature sensing by liquid-liquid phase separation of phytochrome B. *Mol. Cell* **82**, 3015-3029 (2022).

Cheng, Y., Qin, G., Dai, X., & Zhao, Y. NPY genes and AGC kinases define two key steps in auxin-mediated organogenesis in Arabidopsis. *Proc. Natl. Acad. Sci. USA* **105**, 21017-21022 (2008).

Chini, A., et al. The JAZ family of repressors is the missing link in jasmonate signalling. *Nature* **448**, 666-671 (2007).

de Ollas, C., & Dodd, I.C. Physiological impacts of ABA–JA interactions under water-limitation. *Plant Mol. Biol.* **91**, 641-650 (2016).

Fan, W., et al. Arabidopsis PLANT U-BOX44 down-regulates osmotic stress signaling by mediating Ca^{2+}-DEPENDENT PROTEIN KINASE4 degradation. *Plant Cell* **35**, 3870-3888 (2023).

Fernandez-Calvo, P., et al. The Arabidopsis bHLH transcription factors MYC3 and MYC4 are targets of JAZ repressors and act additively with MYC2 in the activation of jasmonate responses. *Plant Cell* **23**, 701-715 (2011).

Fernandez-Milmanda, G.L., et al. A light-dependent molecular link between competition cues and defence responses in plants. *Nat. Plants* **6**, 223-230 (2020).

Foreman, J., et al. Light receptor action is critical for maintaining plant biomass at warm ambient temperatures. *Plant J.* **65**, 441-452 (2011).

Frangedakis, E., et al. MYB-related transcription factors control chloroplast biogenesis. *Cell* **187**, 4859-4876 (2024).

He, Y., Fukushige, H., Hildebrand, D.F., & Gan, S. Evidence supporting a role of jasmonic acid in Arabidopsis leaf senescence. *Plant Physiol.* **128**, 876-884 (2002).

Hong, J., et al. Reframing agriculture by light: the role of light-mediated jasmonates/salicylic acid regulation in plant defense, development and beyond. *Veg. Res.* **4**, e027 (2024).

Hu, S., Yu, K., Yan, J., Shan, X., & Xie, D. Jasmonate perception: ligand-receptor interaction, regulation, and evolution. *Mol. Plant* **16**, 23-42 (2023).

Huai, J., et al. JASMONATE ZIM-domain protein 3 regulates photomorphogenesis and thermomorphogenesis through inhibiting PIF4 in Arabidopsis. *Plant Physiol.* **195**, 2274-2288 (2024).

Huai, J., et al. SEUSS and PIF4 coordinately regulate light and temperature signaling pathways to control plant growth. *Mol. Plant* **11**, 928-942 (2018).

Jing, Y., Guo, Q., & Lin, R. The SNL-HDA19 histone deacetylase complex antagonizes HY5 activity to repress photomorphogenesis in Arabidopsis. *New Phytol.* **229**, 3221-3236 (2020).

Jung, et al. Phytochromes function as thermosensors in Arabidopsis. *Science* **354**, 886-889 (2016).

Kim, C., et al. High ambient temperature accelerates leaf senescence via phytochrome-interacting factor 4 and 5 in Arabidopsis. *Mol. Cells* **43**, 645-661 (2020).

Kim, H.J., Nam, H.G., & Lim, P.O. Regulatory network of NAC transcription factors in leaf senescence. *Curr. Opin. Plant Biol.* **33**, 48-56 (2016).

Klose, C., Nagy, F., & Schäfer, E. Thermal reversion of plant phytochromes. *Mol. Plant* **13**, 386-397 (2020).

Koini, M.A., et al. High temperature-mediated adaptations in plant architecture require the bHLH transcription factor PIF4. *Curr. Biol.* **19**, 408-413 (2009).

Legris, et al. Phytochrome B integrates light and temperature signals in Arabidopsis. *Science* **354**, 897-900 (2016).

Leivar, P., & Quail, P.H. PIFs: pivotal components in a cellular signaling hub. *Trends Plant Sci.* **16**, 19-28 (2011).

Li, C., et al. Jasmonate signaling pathway modulates plant defense, growth, and their trade-offs. *Int. J. Mol. Sci.* **23**, 3945 (2022a).

Li, J.Y., Yang, C., Tian, Y.Y., & Liu, J.X. Regulation of chloroplast development and function at adverse temperatures in plants. *Plant Cell Physiol.* **63**, 580-591 (2022b).

Li, J., Li, G., Wang, H., & Wang Deng, X. W. Phytochrome signaling mechanisms. *Arabidopsis Book* **9**, e0148 (2011).

Li, Y., Du, Y., Huai, J., Jing, Y., & Lin, R. The RNA helicase UAP56 and the E3 ubiquitin ligase COP1 coordinately regulate alternative splicing to repress photomorphogenesis in Arabidopsis. *Plant Cell* **34**, 4191-4212 (2022c).

Li, Y., et al. Regulatory and retrograde signaling networks in the chlorophyll biosynthetic pathway. *J. Integr. Plant Biol.* **67**, 887-911 (2025).

Li, Y., et al. Arabidopsis EXECUTER1 interacts with WRKY transcription factors to mediate plastid-to-nucleus singlet oxygen signaling. *Plant Cell* **35**, 827-851 (2023).

Lin, R., et al. Transposase-derived transcription factors regulate light signaling in Arabidopsis. *Science* **318**, 1302-1305 (2007).

Liu, L., et al. Metabolomics and transcriptomics analysis revealed the response mechanism of alfalfa to combined cold and saline-alkali stress. *Plant J.* **119**, 1900-1919 (2024).

Liu, S., et al. FHY3 interacts with phytochrome B and regulates seed dormancy and germination. *Plant Physiol.* **187**, 289-302 (2021).

Liu, X., Li, Y., & Zhong, S. Interplay between light and plant hormones in the control of Arabidopsis seedling chlorophyll biosynthesis. *Front. Plant Sci.* **8**, 1433 (2017).

Lobell, D.B., Schlenker, W., & Costa-Roberts, J. Climate trends and global crop production since 1980. *Science* **333**, 616-620 (2011).

Moreno, J.E., Tao, Y., Chory, J., & Ballare, C.L. Ecological modulation of plant defense via phytochrome control of jasmonate sensitivity. *Proc. Natl. Acad. Sci. USA* **106**, 4935-4940 (2009).

Noir, S., et al. Jasmonate controls leaf growth by repressing cell proliferation and the onset of endoreduplication while maintaining a potential stand-by mode. *Plant Physiol.* **161**, 1930-1951 (2013).

O'Malley, Ronan C., et al. Cistrome and epicistrome features shape the regulatory DNA landscape. *Cell* **165**, 1280-1292 (2016).

Ortigosa, A., et al. The JA-pathway MYC transcription factors regulate photomorphogenic responses by targeting HY5 gene expression. *Plant J.* **102**, 138-152 (2020).

Oyama, T., Shimura, Y., & Okada, K. The Arabidopsis HY5 gene encodes a bZIP protein that regulates stimulus-induced development of root and hypocotyl. *Genes Dev.* **11**, 2983-2995 (1997).

Park, Y.J., Lee, H.J., Ha, J.H., Kim, J.Y., & Park, C.M. COP1 conveys warm temperature information to hypocotyl thermomorphogenesis. *New Phytol.* **215**, 269-280 (2017).

Qi, T., et al. Regulation of jasmonate-induced leaf senescence by antagonism between bHLH subgroup IIIe and IIId factors in Arabidopsis. *Plant Cell* **27**, 1634-1649 (2015).

Quint, M., et al. Molecular and genetic control of plant thermomorphogenesis. *Nat. Plants* **2**, 15190 (2016).

Rashotte, A.M., et al. A subset of Arabidopsis AP2 transcription factors mediates cytokinin responses in concert with a two-component pathway. *Proc. Natl. Acad. Sci. USA* **103**, 11081-11085 (2006).

Reed, J.W., Nagpal, P., Poole, D.S., Furuya, M., & Chory, J. Mutations in the gene for the red/far-red light receptor phytochrome B alter cell elongation and physiological responses throughout Arabidopsis development. *Plant Cell* **5**, 147-157 (1993).

Sakuraba, Y., et al. Phytochrome-interacting transcription factors PIF4 and PIF5 induce leaf senescence in Arabidopsis. *Nat. Commun.* **5**, 4636 (2014).

Song, C., et al. The multifaceted roles of MYC2 in plants: toward transcriptional reprogramming and stress tolerance by jasmonate signaling. *Front Plant Sci.* **13**, 868874 (2022).

Suzuki, A., et al. *Lotus japonicus* nodulation is photomorphogenetically controlled by sensing the red/far red (R/FR) ratio through jasmonic acid (JA) signaling. *Proc. Natl. Acad. Sci. USA* **108**, 16837-16842 (2011).

Thines, B., et al. JAZ repressor proteins are targets of the SCF^{COI1} complex during jasmonate signalling. *Nature* **448**, 661-665 (2007).

Toledo-Ortiz, G., et al. The HY5-PIF regulatory module coordinates light and temperature control of photosynthetic gene transcription. *PLoS Genet.* **10**, e1004416 (2014).

Varshney, V., et al. The Arabidopsis F-box protein SKP1-INTERACTING PARTNER 31 modulates seed maturation and seed vigor by targeting JASMONATE ZIM DOMAIN proteins independently of jasmonic acid-isoleucine. *Plant Cell* **35**, 3712-3738 (2023).

Wang, Y., Mostafa, S., Zeng, W., & Jin, B. Function and mechanism of jasmonic acid in plant responses to abiotic and biotic Stresses. *Int. J. Mol. Sci*. **22**, 8568 (2021).

Wu, S., et al. The MYC2-PUB22-JAZ4 module plays a crucial role in jasmonate signaling in tomato. *Mol. Plant* **17**, 598-613 (2024).

Xiao, Y., et al. HY5: a pivotal regulator of light-dependent development in higher plants. *Front. Plant Sci.* **12**, 800989 (2022).

Xu, H., et al. The JA-to-ABA signaling relay promotes lignin deposition for wound healing in Arabidopsis. *Mol. Plant* **17**, 1594-1605 (2024a).

Xu, L., et al. The SCF(COI1) ubiquitin-ligase complexes are required for jasmonate response in Arabidopsis. *Plant Cell* **14**, 1919-1935 (2002).

Xu, X., Hu, J., & Yuan, Z. Stabilization or degradation? post-translational modifications of JAZ proteins in plants. *Mol. Plant* **17**, 1002-1004 (2024b).

Xu, X., et al. Convergence of light and chloroplast signals for de-etiolation through ABI4-HY5 and COP1. *Nat. Plants* **2**, 16066 (2016).

Yan, J., et al. The Arabidopsis F-box protein CORONATINE INSENSITIVE1 is stabilized by SCF^{COI1} and degraded via the 26S proteasome pathway. *Plant Cell* **25**, 486-498 (2013).

Yang, C., et al. HY5-HDA9 module transcriptionally regulates plant autophagy in response to light-to-dark conversion and nitrogen starvation. *Mol. Plant* **13**, 515-531 (2020).

Zhang, D., Jing, Y., Jiang, Z., & Lin, R. The chromatin-remodeling factor PICKLE integrates brassinosteroid and gibberellin signaling during skotomorphogenic growth in Arabidopsis. *Plant Cell* **26**, 2472-2485 (2014).

Zhang, D., Li, Y., Zhang, X., Zha, P., & Lin, R. The SWI2/SNF2 chromatin-remodeling ATPase BRAHMA regulates chlorophyll biosynthesis in Arabidopsis. *Mol. Plant* **10**, 155-167 (2017).

Zhang, T., et al. GLK transcription factors accompany ELONGATED HYPOCOTYL5 to orchestrate light-induced seedling development in Arabidopsis. *Plant Physiol.* **194**, 2400-2421 (2024).

Zhang, Y., Liu, Z., Chen, Y., He, J.X., & Bi, Y. PHYTOCHROME-INTERACTING FACTOR 5 (PIF5) positively regulates dark-induced senescence and chlorophyll degradation in Arabidopsis. *Plant Sci.* **237**, 57-68 (2015).

Zhao, C., et al. Temperature increase reduces global yields of major crops in four independent estimates. *Proc. Natl. Acad. Sci. USA* **114**, 9326-9331 (2017).

Zhou, Y., et al. NPR1 promotes blue light-induced plant photomorphogenesis by ubiquitinating and degrading PIF4. *Proc. Natl. Acad. Sci. USA* **121**, e2412755121 (2024).

Zhu, T., et al. Warm temperature triggers JOX and ST2A-mediated jasmonate catabolism to promote plant growth. *Nat. Commun.* **12**, 4804 (2021).

Zhu, X., et al. Jasmonic acid promotes degreening via MYC2/3/4- and ANAC019/055/072-mediated regulation of major chlorophyll catabolic genes. *Plant J.* **84**, 597-610 (2015).

Acknowledgements

We thank Dr. Daoxin Xie (Tsinghua University) for providing *coi1-8* mutant, Dr. Chuanyou Li (Shandong Agricultural University) for providing *35S:MYC2-Myc* seeds, and Dr. Lei Wang (Institute of Botany, Chinese Academy of Sciences) for providing *myc2-2* and *myc2/3/4* seeds. This work was supported by grants from the Key Research and Development Program of Zhejiang Province (2024SSYS0100 to R.L.), National Key Research and Development Program of China (2024YFA1306702 to J.H.), National Natural Science Foundation of China (U25A20633 and 32030009 to R.L., 32270262 to J.H.), and Project of Stable Support for Youth Teams in Basic Research of the Chinese Academy of Sciences (YSBR-119 to J.H.).

Author contributions

P.Q. performed most of the experiments, analyzed data, and wrote the manuscript; J.H. generated plant materials, analyzed data, discussed the project, and wrote the manuscript; N.G. and Y.Y. conducted part of experiments and material preparation; R.L. conceived and supervised the study, analyzed data, and revised the paper.

Competing interests

The authors declare no competing interests.

Figure Legends

Fig. 1 Warm temperature and JA collaboratively regulate cotyledon and chloroplast development.

a Phenotype of Col-0 seedlings grown for 6 days on MS medium (with or without 25 μM MeJA) under continuous white light at either 22°C or 28°C. **b** Quantification of cotyledon area of seedlings shown in (**a**). *n*= ~ 50. **c** Chlorophyll contents. The means and SD were obtained from three biological replicates. Different letters denote statistically significant differences as determined by two-way ANOVA followed by Tukey's multiple comparison test ($p < 0.05$). **d** Representative FluorCam false color images. Color scale (0 to 1) represents signal intensity. **e** Maximum efficiency of photosystem II (Fv/Fm). *n* = 15. Data were visualized with box plots displaying the median (center line), the interquartile range (IQR; box bounds from the 25th to 75th percentiles), and whiskers extending to the minimum and maximum values within 1.5× IQR of the quartiles. Points beyond the whiskers are shown individually and considered outliers. **f** Confocal laser scanning microscopy images showing chlorophyll autofluorescence (magenta). The experiments were repeated at least three times independently and yielded similar results (**d** and **f**). **g** Transmission electron microscopy images of chloroplasts (magnification 6,000×). Enlarged regions (dashed boxes) highlight grana stacks (white brackets) (magnification 15,000×). sg, starch granule; gt, grana thylakoid; st, stroma thylakoid; pg, plastoglobulus. **h** Chloroplast number per cell shown in (**f**). *n* = 50. **i** Chloroplast area shown in (**f**). *n* = 500. **j** Chlorophyll fluorescence intensity shown in (**f**). *n* = 500. **k** Thylakoid stacking number per granum shown in (**g**). *n* = ~ 50. The data was visualized with violin plots. Solid lines in the center represent the median, and small circles represent minimum-maximum distribution of the data (**b**, and **h-k**). The means and SD were obtained from biologically independent samples and precise values of replicates (*n*) for each data are provided in Source data file. Different letters denote statistically significant differences as determined by two-way ANOVA followed by Tukey's multiple comparison test ($p < 0.05$) (**b**, **e** and **h-k**).

Fig. 2 phyB and COI1 play opposite roles in regulating cotyledon chlorosis.

a Cotyledon phenotype of different genotypes grown for 6 days on medium (with or without 25 μM MeJA) under continuous white light at either 22℃ or 28℃. **b** Chlorophyll contents. The means and SD were obtained from three biological replicates. Different letters denote statistically significant differences as determined by two-way ANOVA followed by Tukey's multiple comparison test ($p < 0.05$). **c** Representative FluorCam false color images of seedlings grown at the 28℃+MeJA condition. **d** Fv/Fm. n =15. Data were visualized with box plots displaying the median (center line), the interquartile range (IQR; box bounds from the 25th to 75th percentiles), and whiskers extending to the minimum and maximum values within 1.5×IQR of the quartiles. Points beyond the whiskers are shown individually and considered outliers. **e** Confocal laser scanning microscopy images showing chlorophyll autofluorescence (magenta). The experiments were repeated at least three times independently and yielded similar results (**c** and **e**). **f** Chloroplast area shown in (**e**). n = ~ 500. **g** Chloroplast number per cell shown in (**e**). n = ~ 50. **h** Chlorophyll fluorescence intensity shown in (**e**). n = ~ 500. The data was visualized with violin plots. Solid lines in the center represent the median, and small circles represent minimum-maximum distribution of the data (**f**-**h**). The means and SD were obtained from biologically independent samples and precise values of replicates (n) for each data are provided in Source data file. Different letters denote statistically significant differences as determined by two-way ANOVA followed by Tukey's multiple comparison test ($p < 0.05$) (**d**, and **f**-**h**).

Fig. 3 phyB physically interacts with JAZ1 and JAZ3.

a Yeast two-hybrid assay. Full-length (FL) phyB and its truncated fragments (C651 and C451) were fused to the GAL4 activation domain (GAD). JAZ1 and JAZ3 were fused to the GAL4 DNA-binding domain (GBD). -WL, medium lacking Trp and Leu; -WLHA, medium lacking Trp, Leu, His and Ade. **b** LCI assay. JAZ1 and JAZ3 were fused to the N-terminal firefly LUC; phyB was fused to the C-terminal LUC. The different combinations of constructs were co-transformed into *N. benthamiana* leaves. The luminescence was monitored after 2 days of dark growth. **c** BiFC assay. phyB was fused to the N-terminus of YFP; JAZ1 and JAZ3 were fused to the C-terminus of

YFP. The constructs were co-transformed into Arabidopsis protoplasts and fluorescence was observed using a confocal microscope. **d** and **e** Co-IP assay. Transgenic plants expressing *35S:JAZ1-GFP* (**d**) or *35S:JAZ3-GFP* (**e**) or together with *35S:Myc-phyB* were grown under white light at 22℃ for 6 days and then transferred to 28℃ for 3 hours. Protein extracts were immunoprecipitated using an anti-GFP antibody, followed by immunoblotting with anti-GFP or anti-Myc antibodies. The values indicate the relative intensities of the GFP or Myc immunoblot signals, each normalized to its respective Actin loading control. The relative protein levels at 22℃ were defined as 1.0. **f** and **g** *In vitro* pull-down assay. Recombinant proteins of His-JAZ1 (**f**) or His-JAZ3 (**g**) were incubated GST-phyB-C1 (or GST) and pulled down with Glutathione Sepharose 4B beads, and then detected by immunoblotting with anti-GST or anti-His antibodies. The experiments were repeated at least twice and yielded similar results (**b**-**g**).

Fig. 4 phyB affects JAZ1 protein ubiquitination and stability.

a and **b** *In vivo* ubiquitination assay of JAZ1 at 22℃ (**a**) or 28℃ (**b**). After being grown for 6 days at either 22℃ or 28℃, the *35S:JAZ1-GFP* and *35S:JAZ1-GFP phyB-9* seedlings were then treated with 100 μM MeJA + 50 μM Btz for 3 h at their respective temperatures. The values indicate relative intensities of the anti-UBQ11 bands normalized to the anti-Actin control. The relative protein abundance in the mock-treated *35S:JAZ1-GFP* samples was defined as 1.0 for normalization. **c** and **e** Immunoblotting of JAZ1-GFP protein upon MeJA treatment at either 22℃ (**c**) or 28℃ (**e**). The seedlings were grown for 6 days and then treated with 100 μM MeJA (with or without 50 μM MG132) for 6 h. Anti-Actin served as loading controls. **d** and **f** Time-course of JAZ1 degradation at either 22℃ (**d**) or 28℃ (**f**). Six-day-old seedlings were treated with 100 μM MeJA for specified durations at the respective growth temperatures. Proteins were immunoblotted with anti-GFP and anti-Actin (control) antibodies. The values represent the relative intensities of the GFP signals, normalized to the corresponding Actin loading controls (**c**-**f**). The signal in the *35S:JAZ1-GFP* samples at time zero (**c** and **e**) or under mock treatment (**d** and **f**) was defined as 1.0. The experiments were repeated at least twice and yielded similar results.

Fig. 5 HY5 and MYCs oppositely regulate cotyledon yellowing.

a Cotyledon phenotype of different seedlings grown for 6 days on medium (with or without 25 μM MeJA) under continuous white light at either 22℃ or 28℃. **b** Chlorophyll contents. The means and SD were obtained from three biological replicates. Different letters denote statistically significant differences as determined by two-way ANOVA followed by Tukey's multiple comparison test ($p < 0.05$). **c** FluorCam false color images. Color scale (0 to 1) represents signal intensity. **d** Fv/Fm. n =12. Data were visualized with box plots displaying the median (center line), the interquartile range (IQR; box bounds from the 25th to 75th percentiles), and whiskers extending to the minimum and maximum values within 1.5×IQR of the quartiles. Points beyond the whiskers are shown individually and considered outliers. **e** Confocal microscopy images showing chlorophyll autofluorescence (magenta). The experiments were repeated at least three times independently and yielded similar results (**c** and **e**). **f** Transmission electron micrographs of chloroplast ultrastructure (magnification 6,000×). Enlarged areas (dashed boxes) highlight grana stacks (white brackets) (magnification 15,000×). sg, starch granules; gt, grana thylakoid; st, stroma thylakoid; pg, plastoglobulus. **g** Chloroplast number per cell shown in (**e**). n = ~ 50. **i** Chloroplast area shown in (**e**). n = ~ 500. **h** Chlorophyll fluorescence intensity shown in (**e**). n = ~ 500. The data was visualized with violin plots. Solid lines in the center represent the median, and small circles represent minimum-maximum distribution of the data (**g-i**). The means and SD were obtained from biologically independent samples and precise values of replicates (n) for each data are provided in Source data file. Different letters denote statistically significant differences as determined by two-way ANOVA followed by Tukey's multiple comparison test ($p < 0.05$) (**d**, and **g-i**).

Fig. 6 Transcriptional profiling of genes differentially regulated by HY5 and MYCs.

a Number of DEGs in *hy5-215* versus Col-0 under the 28℃+MeJA condition. **b** The volcano plot diagram depicts the expression levels of DEGs from (**a**). **c** Number of DEGs in *myc2/3/4* versus

Col-0 under the 28℃+MeJA condition. **d** The volcano plot diagram depicts the expression levels of DEGs from (**c**). Red point represent upregulated DEGs (Log2FC ≥1, FDR < 0.05) and blue point represent downregulated DEGs (Log2FC ≤1, FDR < 0.05) (**b** and **d**). **e** GO analysis of HY5 positively regulated genes. **f** GO analysis of MYCs positively regulated genes. David online database (https://david.ncifcrf.gov/conversion.jsp) was used to perform Gene Ontology (GO) clustering analysis, followed by GO enrichment based on specific cellular component or biological process. Top 10 GO terms were selected and visualized with bubble chart. The bubble size is proportional to the number of DEGs, the bubble color represents -Log10 FDR value, and the horizontal axis indicates the relative ratio to all genes within that GO category (**e** and **f**).

Fig. 7 Genome-wide profiling of HY5 and MYC2 binding sites through DNA affinity purification sequencing.

a Heatmap of HY5-binding peaks enriched near the transcription start site (TSS) of two technical replicates. **b** Distribution profile of MYC2 binding sites relative to TSS. **c** DNA logo of the significant enriched motif within the HY5 binding peaks. **d** DNA logo of the significant enriched motif within the MYC2 binding peaks. The CACGTG motif shows up as the most enriched core sequence. The E-value was calculated by MEME (**c** and **d**). **e** Enrichment of HY5 targets in cotyledon development genes. **f** Enrichment of HY5 targets in stress and hormone signaling pathways. **g** Enrichment of MYC2 targets in leaf development and JA-responsive genes. Heatmap shows DAP-seq fold enrichment versus input control (**e**-**g**).

Fig. 8 Transcriptional regulation of chloroplast development-related genes by HY5 and MYC2.

a and **c** Schematic diagram of the promoter of *GLK1* (**a**) and *RAP2.6* (**c**). G-box (blue oval); G-box-like element (green oval); Z-box (red oval); P1-P3, ChIP amplicons. **b** ChIP-qPCR showing HY5 enrichment at the *GLK1* promoter region. **d** ChIP-qPCR showing MYC2 enrichment at the *RAP2.6* promoter region. Transgenic seedlings expressing *35S:HY5-GFP* or *35S:MYC2-Myc* were

grown under three different conditions for 6 days. Relative enrichment was determined as the percentage of input DNA, calculated by normalizing the ChIP signal against the input control. *ACTIN7* was used as the control gene. IgG, Immunoglobulin G. The means and SD were obtained from three technical replicates. Different letters denote statistically significant differences as determined by two-way ANOVA followed by Tukey's multiple comparison test ($p < 0.05$) (**b** and **d**). **e** and **g** Schematic diagrams of reporter and effector constructs for the transient expression assay. **f** and **h** Dual-luciferase assay showing the transcriptional activity of either HY5 (**f**) or MYC2 (**h**) on the respective promoters. Relative activity was expressed as the ratio of LUC to REN. The means and SD were obtained from biologically independent samples ($n = 3$). Different letters denote statistically significant differences as determined by two-way ANOVA followed by Tukey's multiple comparison test ($p < 0.05$). The experiments were repeated at least twice and yielded similar results (**f** and **h**).

Fig. 9 A working model.

Under normal growth temperature conditions (22℃), phyB interacts with and stabilizes JAZ proteins (e.g., JAZ1 and JAZ3), thereby suppressing the activity of MYC transcription factors such as MYC2. Consequently, MYC2 only weakly induces the expression of downstream genes related to chlorosis and stress response, such as *RAP2.6*. Simultaneously, phyB photoreceptor transmits light signals to the HY5 transcription factor, which promotes the expression of genes involved in cotyledon development and chloroplast biogenesis (e.g., *GLK1*), thereby sustaining normal growth and development. Under the combined 28℃+MeJA condition, reduced phyB activity (less Pfr form) leads to two major outcomes: first, it weakens the interaction with JAZ proteins, which are subsequently degraded via the JA-triggered, COI1-mediated ubiquitination pathway, resulting in the release of MYC2 and activation of its transcriptional function; second, it lowers protein levels and activity of HY5 (Park et al., 2017). Together, these effects contribute to retarded chloroplast development and cotyledon growth.

Editorial Summary:

This paper reports the mechanism by which phytochrome B integrates JA and warm temperature signals in regulating chloroplast development through the HY5-MYCs transcriptional regulatory network.

Peer Review Information: *Nature Communications* thanks Gen-ichiro Arimura and the other anonymous, reviewer(s) for their contribution to the peer review of this work. A peer review file is available."

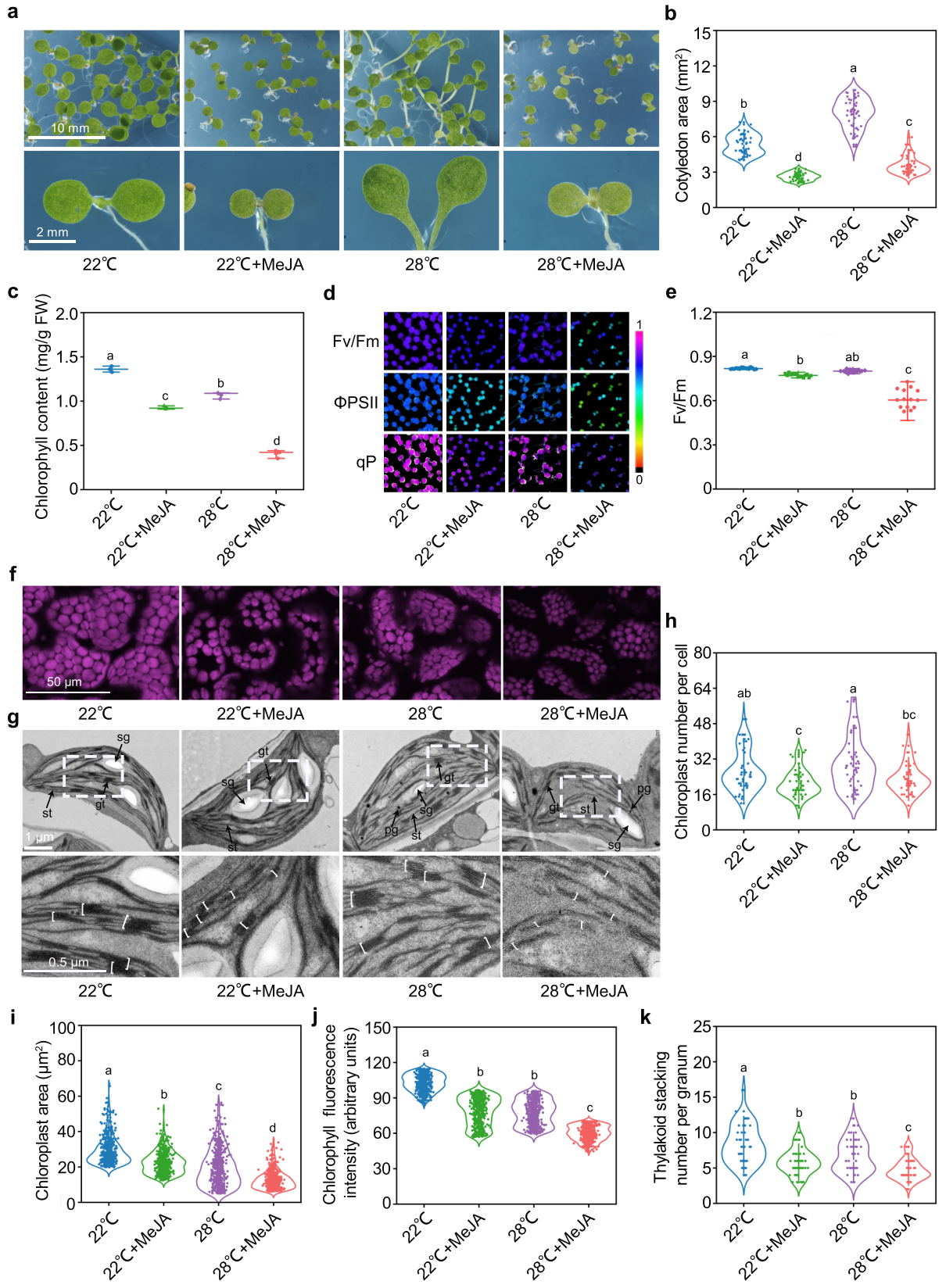
a
10 mm
2 mm
22℃
22℃+MeJA
28℃
28℃+MeJA
b
Cotyledon area (mm²)
c
Chlorophyll content (mg/g FW)
d
Fv/Fm
ΦPSII
qP
e
f
50 μm
g
sg
gt
st
pg
1 μm
0.5 μm
h
Chloroplast number per cell
i
Chloroplast area (μm²)
j
Chlorophyll fluorescence intensity (arbitrary units)
k
Thylakoid stacking number per granum

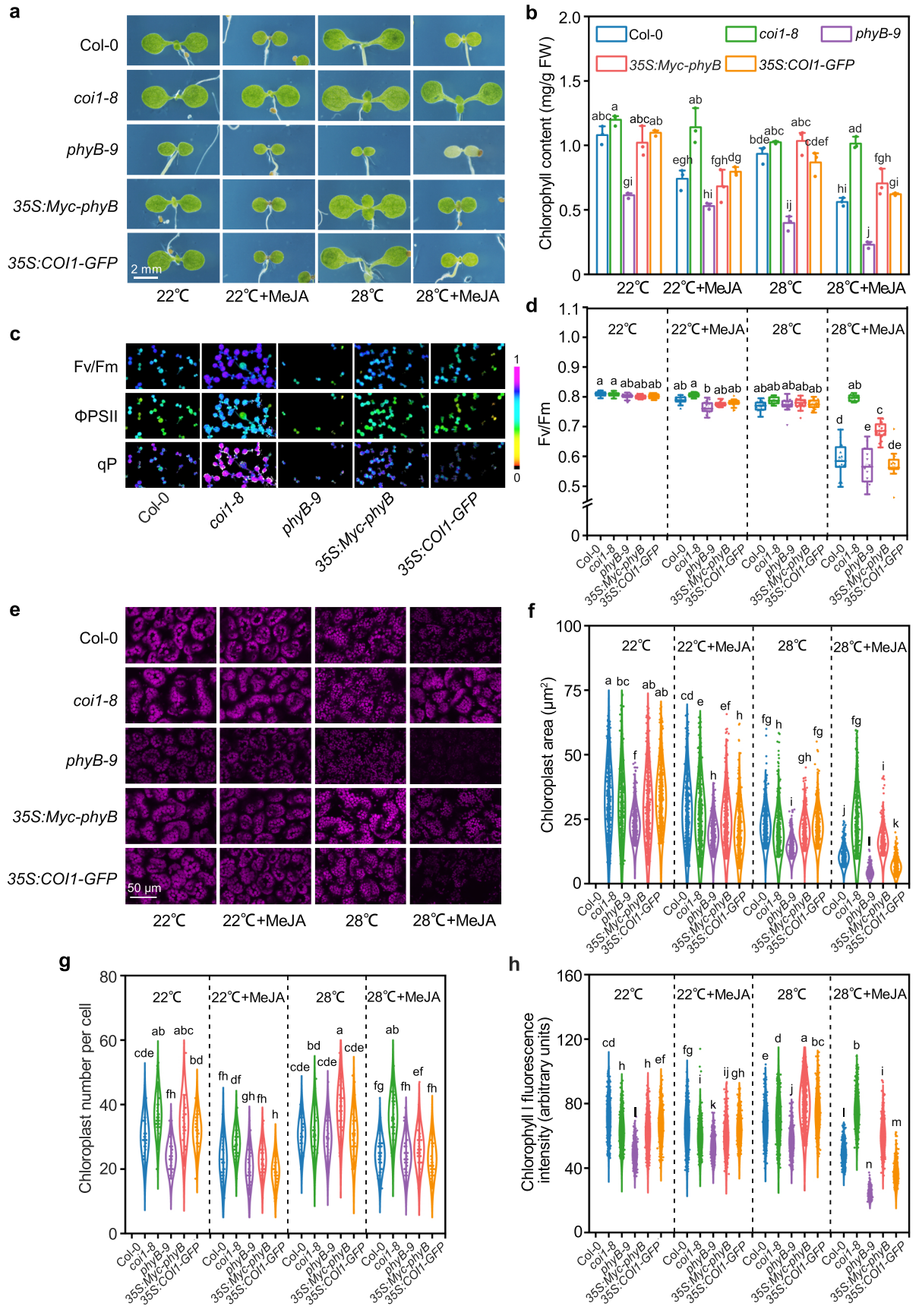
a
Col-0
coi1-8
phyB-9
35S:Myc-phyB
35S:COI1-GFP
2 mm
22℃
22℃+MeJA
28℃
28℃+MeJA
b
Col-0
coi1-8
phyB-9
35S:Myc-phyB
35S:COI1-GFP
Chlorophyll content (mg/g FW)
c
Fv/Fm
ΦPSII
qP
1
0
Col-0
coi1-8
phyB-9
35S:Myc-phyB
35S:COI1-GFP
d
Fv/Fm
e
50 μm
f
Chloroplast area (μm²)
g
Chloroplast number per cell
h
Chlorophyll I fluorescence intensity (arbitrary units)

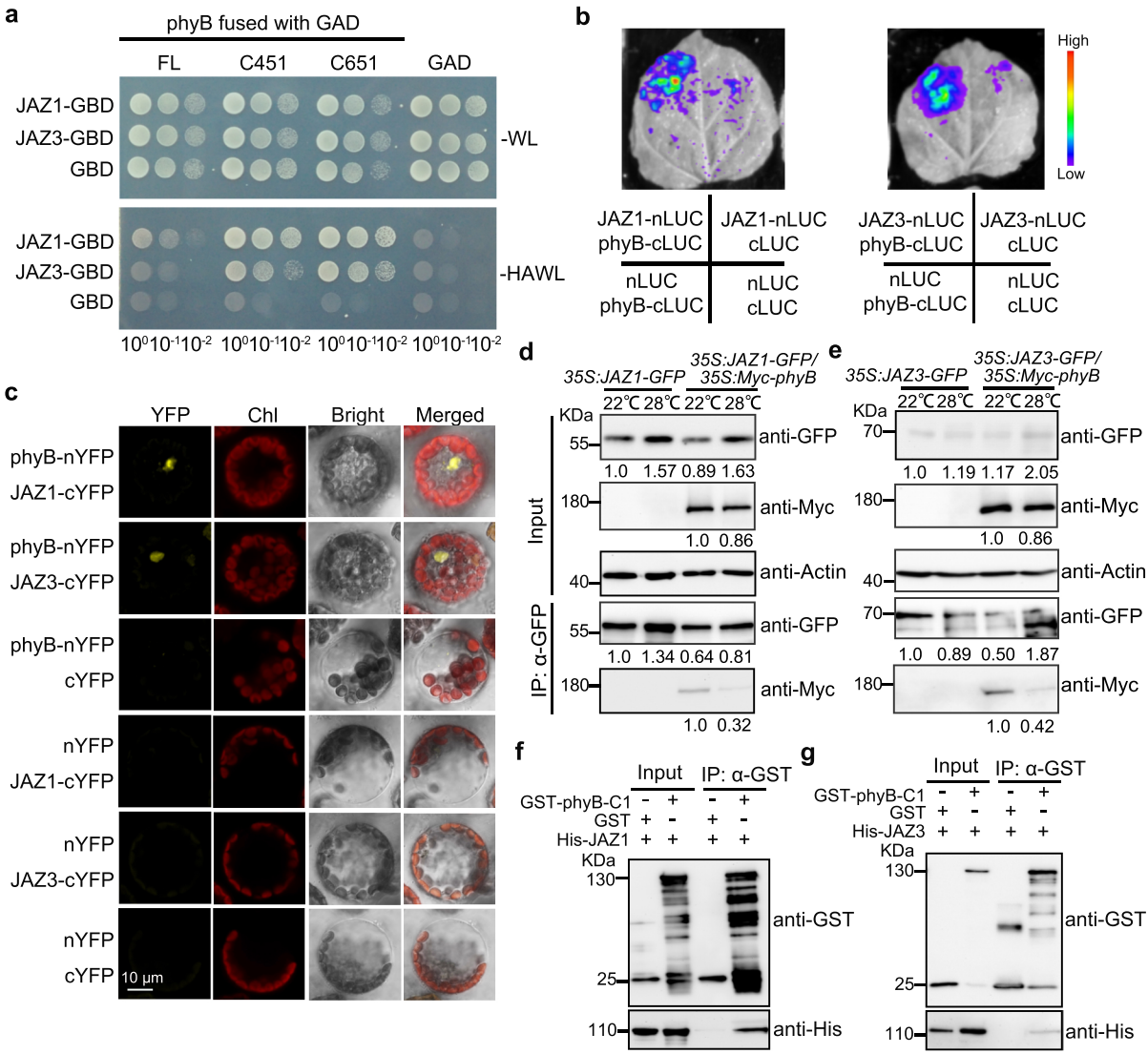
a
phyB fused with GAD
FL
C451
C651
GAD
JAZ1-GBD
JAZ3-GBD
GBD
-WL
-HAWL
10^0 10^-1 10^-2
b
High
Low
JAZ1-nLUC
phyB-cLUC
JAZ1-nLUC
cLUC
nLUC
phyB-cLUC
nLUC
cLUC
JAZ3-nLUC
phyB-cLUC
JAZ3-nLUC
cLUC
nLUC
phyB-cLUC
nLUC
cLUC
c
YFP
Chl
Bright
Merged
phyB-nYFP
JAZ1-cYFP
phyB-nYFP
JAZ3-cYFP
phyB-nYFP
cYFP
nYFP
JAZ1-cYFP
nYFP
JAZ3-cYFP
nYFP
cYFP
10 μm
d
35S:JAZ1-GFP
35S:JAZ1-GFP/
35S:Myc-phyB
22℃ 28℃ 22℃ 28℃
KDa
55
anti-GFP
1.0 1.57 0.89 1.63
Input
180
anti-Myc
1.0 0.86
40
anti-Actin
IP: α-GFP
55
anti-GFP
1.0 1.34 0.64 0.81
180
anti-Myc
1.0 0.32
e
35S:JAZ3-GFP
35S:JAZ3-GFP/
35S:Myc-phyB
22℃ 28℃ 22℃ 28℃
KDa
70
anti-GFP
1.0 1.19 1.17 2.05
180
anti-Myc
1.0 0.86
40
anti-Actin
70
anti-GFP
1.0 0.89 0.50 1.87
180
anti-Myc
1.0 0.42
f
Input
IP: α-GST
GST-phyB-C1 - + - +
GST + - + -
His-JAZ1 + + + +
KDa
130
anti-GST
25
110
anti-His
g
Input
IP: α-GST
GST-phyB-C1 - + - +
GST + - + -
His-JAZ3 + + + +
KDa
130
anti-GST
25
110
anti-His

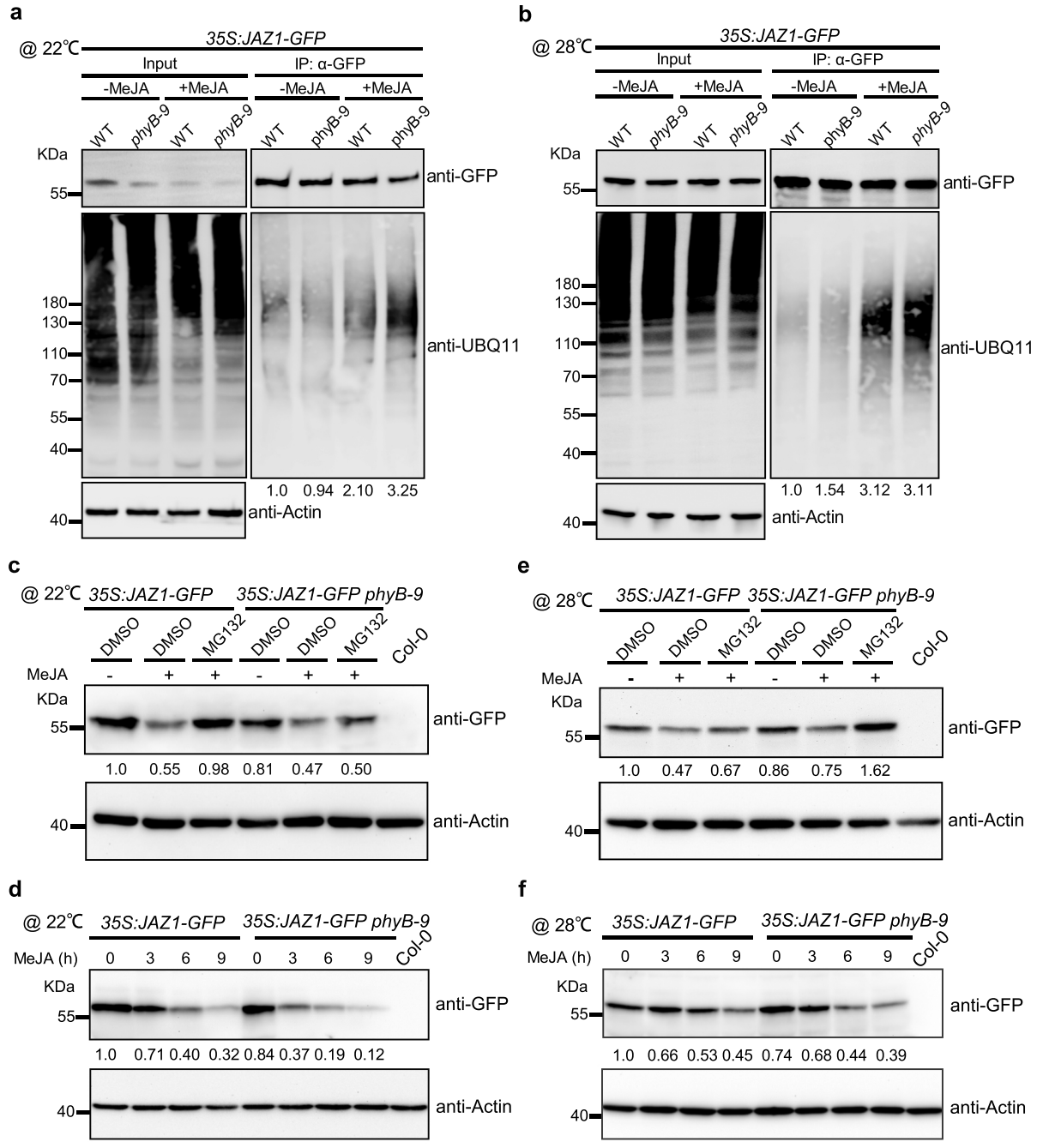
a
@ 22℃
35S:JAZ1-GFP
Input
IP: α-GFP
-MeJA
+MeJA
-MeJA
+MeJA
WT
phyB-9
WT
phyB-9
WT
phyB-9
WT
phyB-9
KDa
55
anti-GFP
180
130
110
70
55
40
anti-UBQ11
1.0 0.94 2.10 3.25
40
anti-Actin
b
@ 28℃
35S:JAZ1-GFP
Input
IP: α-GFP
-MeJA
+MeJA
-MeJA
+MeJA
WT
phyB-9
WT
phyB-9
WT
phyB-9
WT
phyB-9
KDa
55
anti-GFP
180
130
110
70
55
40
anti-UBQ11
1.0 1.54 3.12 3.11
40
anti-Actin
c
@ 22℃
35S:JAZ1-GFP
35S:JAZ1-GFP phyB-9
DMSO
DMSO
MG132
DMSO
DMSO
MG132
Col-0
MeJA
-
+
+
-
+
+
KDa
55
anti-GFP
1.0 0.55 0.98 0.81 0.47 0.50
40
anti-Actin
e
@ 28℃
35S:JAZ1-GFP
35S:JAZ1-GFP phyB-9
DMSO
DMSO
MG132
DMSO
DMSO
MG132
Col-0
MeJA
-
+
+
-
+
+
KDa
55
anti-GFP
1.0 0.47 0.67 0.86 0.75 1.62
40
anti-Actin
d
@ 22℃
35S:JAZ1-GFP
35S:JAZ1-GFP phyB-9
MeJA (h)
0
3
6
9
0
3
6
9
Col-0
KDa
55
anti-GFP
1.0 0.71 0.40 0.32 0.84 0.37 0.19 0.12
40
anti-Actin
f
@ 28℃
35S:JAZ1-GFP
35S:JAZ1-GFP phyB-9
MeJA (h)
0
3
6
9
0
3
6
9
Col-0
KDa
55
anti-GFP
1.0 0.66 0.53 0.45 0.74 0.68 0.44 0.39
40
anti-Actin

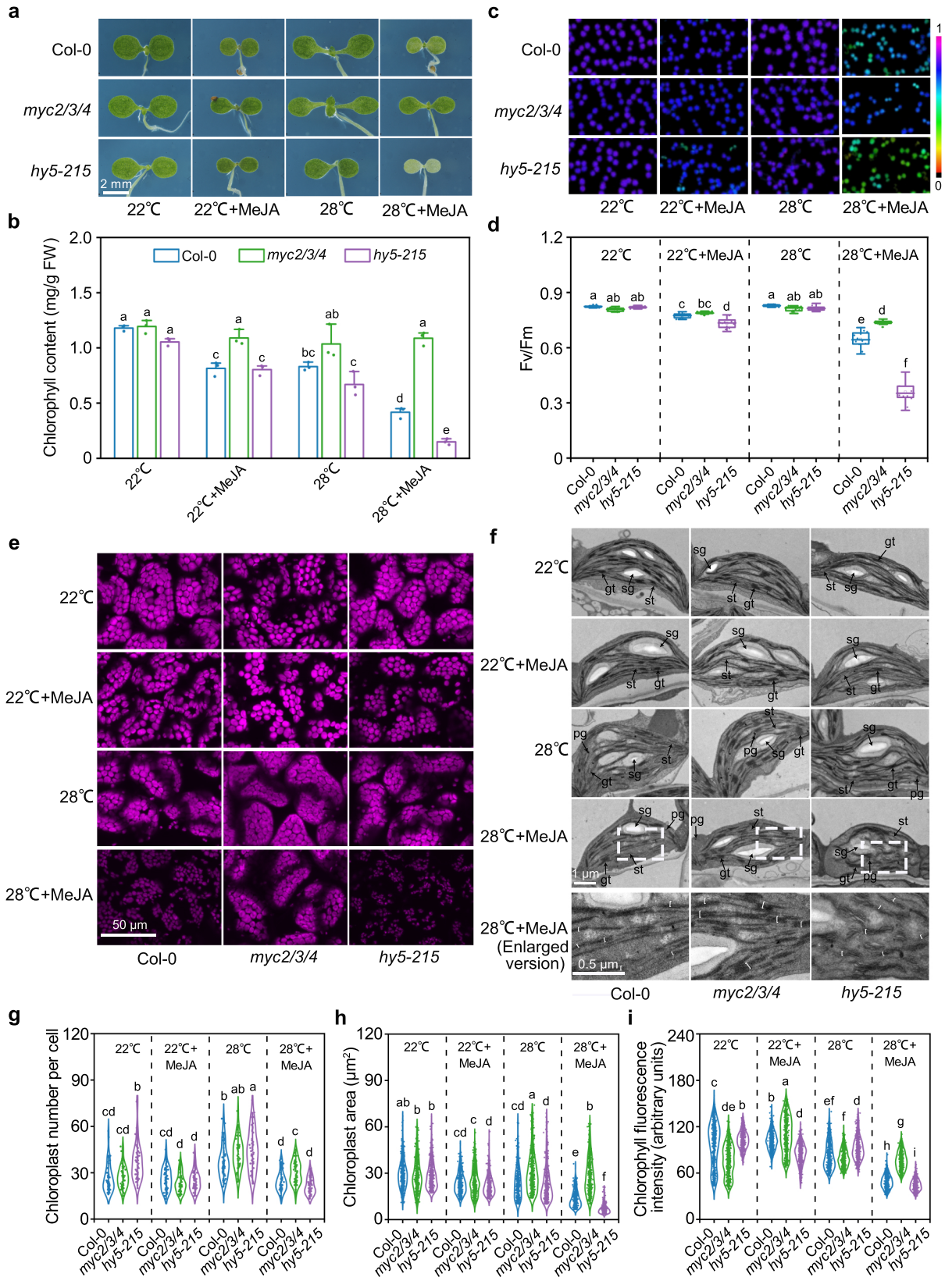
a
Col-0
myc2/3/4
hy5-215
2 mm
22℃
22℃+MeJA
28℃
28℃+MeJA
c
1
0
b
Chlorophyll content (mg/g FW)
Col-0
myc2/3/4
hy5-215
d
Fv/Fm
e
50 μm
f
1 μm
0.5 μm
sg
gt
st
pg
28℃+MeJA (Enlarged version)
g
Chloroplast number per cell
h
Chloroplast area (μm²)
i
Chlorophyll fluorescence intensity (arbitrary units)

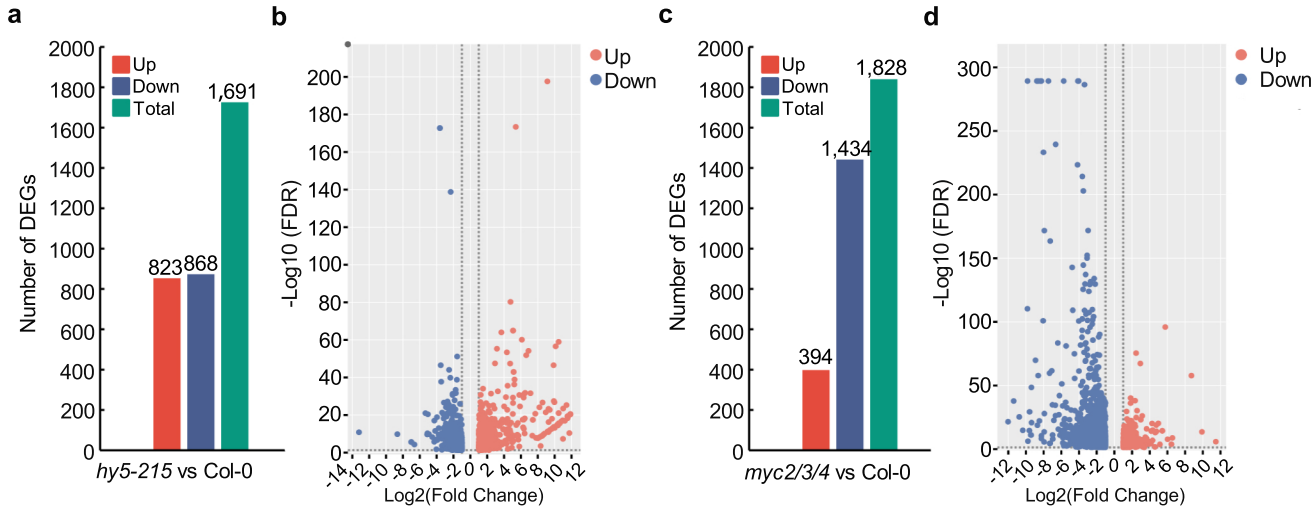
a
Number of DEGs
Up
Down
Total
823
868
1,691
hy5-215 vs Col-0
b
-Log10 (FDR)
Up
Down
Log2(Fold Change)
c
Number of DEGs
Up
Down
Total
394
1,434
1,828
myc2/3/4 vs Col-0
d
-Log10 (FDR)
Up
Down
Log2(Fold Change)

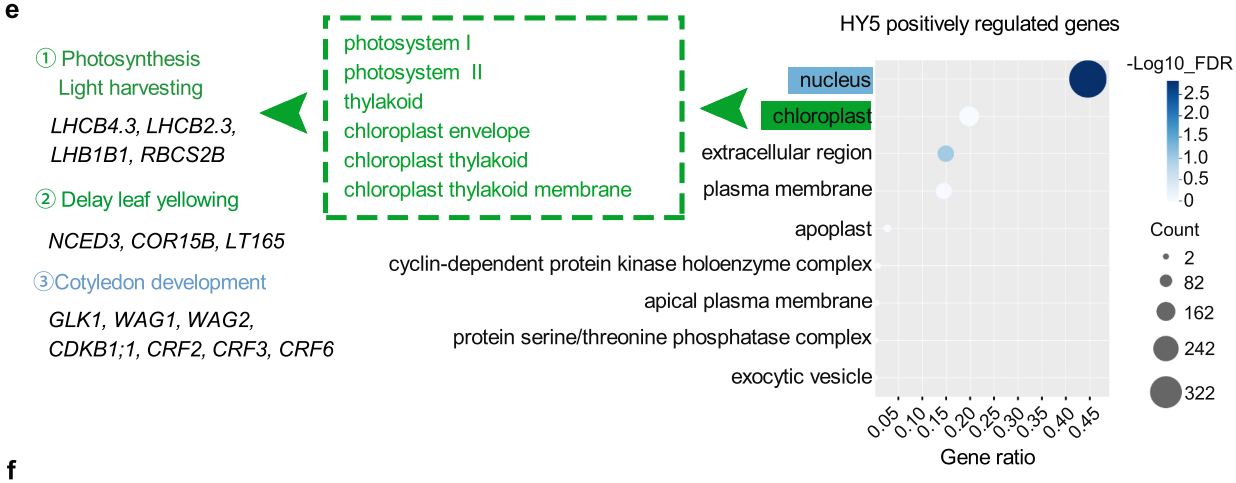
e
① Photosynthesis
Light harvesting
LHCB4.3, LHCB2.3,
LHB1B1, RBCS2B
② Delay leaf yellowing
NCED3, COR15B, LT165
③Cotyledon development
GLK1, WAG1, WAG2,
CDKB1;1, CRF2, CRF3, CRF6
photosystem I
photosystem II
thylakoid
chloroplast envelope
chloroplast thylakoid
chloroplast thylakoid membrane
HY5 positively regulated genes
nucleus
chloroplast
extracellular region
plasma membrane
apoplast
cyclin-dependent protein kinase holoenzyme complex
apical plasma membrane
protein serine/threonine phosphatase complex
exocytic vesicle
Gene ratio
-Log10_FDR
Count

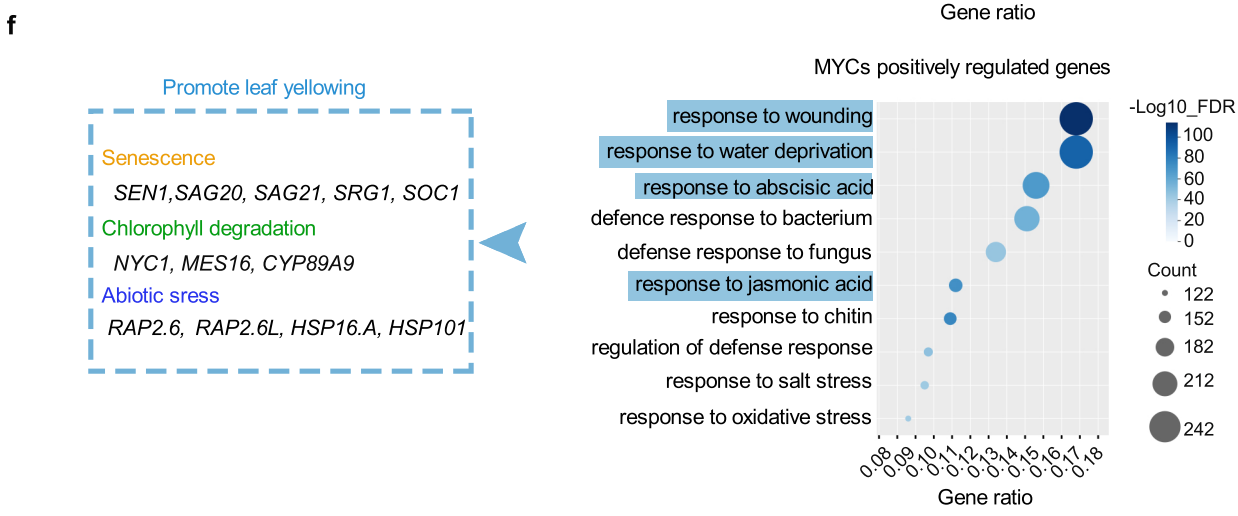
f
Promote leaf yellowing
Senescence
SEN1,SAG20, SAG21, SRG1, SOC1
Chlorophyll degradation
NYC1, MES16, CYP89A9
Abiotic sress
RAP2.6, RAP2.6L, HSP16.A, HSP101
MYCs positively regulated genes
response to wounding
response to water deprivation
response to abscisic acid
defence response to bacterium
defense response to fungus
response to jasmonic acid
response to chitin
regulation of defense response
response to salt stress
response to oxidative stress
Gene ratio
-Log10_FDR
Count

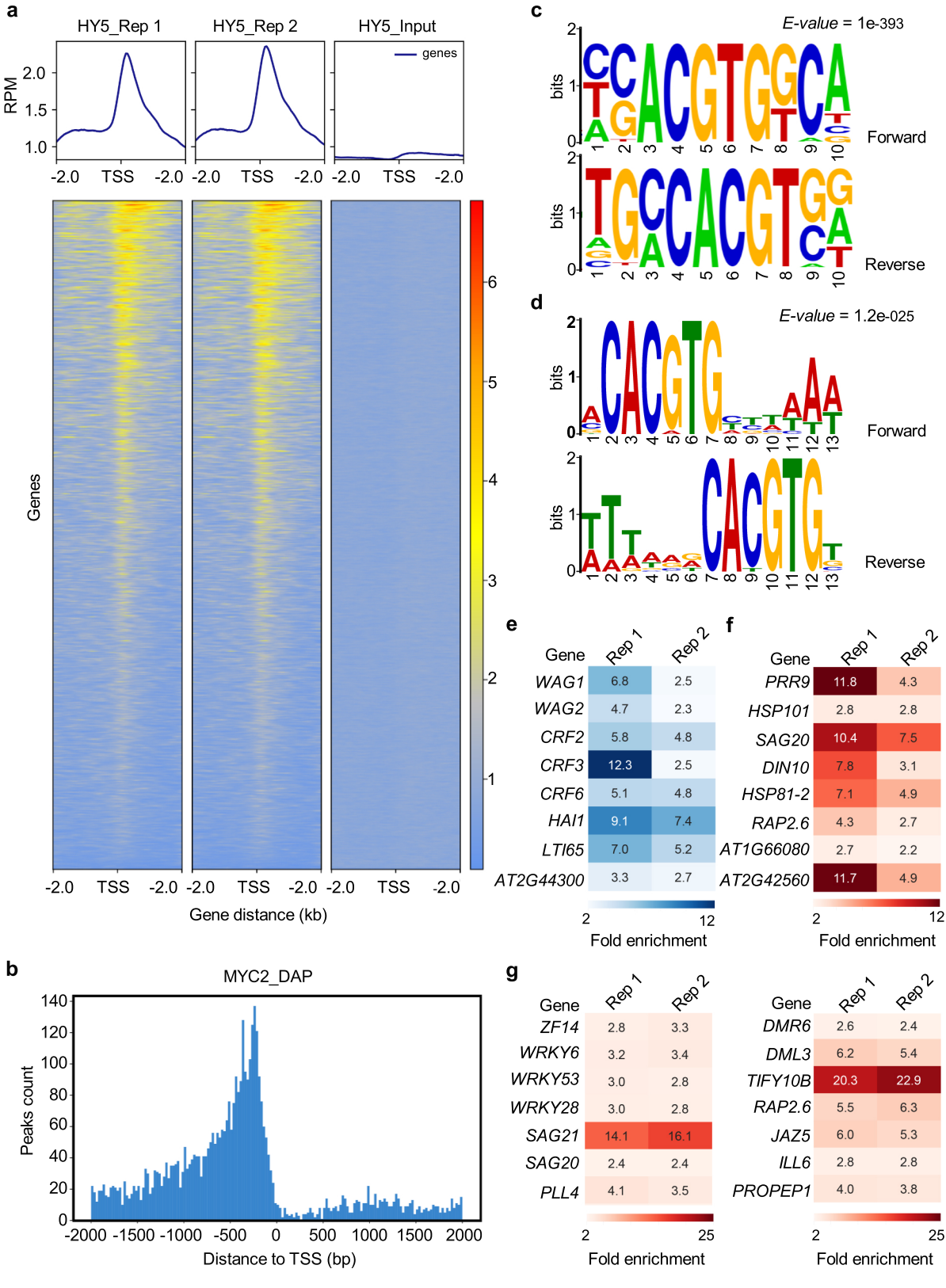
a
HY5_Rep 1
HY5_Rep 2
HY5_Input
genes
RPM
2.0
1.5
1.0
-2.0 TSS -2.0
Genes
Gene distance (kb)
c
E-value = 1e-393
bits
Forward
Reverse
d
E-value = 1.2e-025
e
Gene
Rep 1
Rep 2
WAG1 6.8 2.5
WAG2 4.7 2.3
CRF2 5.8 4.8
CRF3 12.3 2.5
CRF6 5.1 4.8
HAI1 9.1 7.4
LTI65 7.0 5.2
AT2G44300 3.3 2.7
Fold enrichment
f
PRR9 11.8 4.3
HSP101 2.8 2.8
SAG20 10.4 7.5
DIN10 7.8 3.1
HSP81-2 7.1 4.9
RAP2.6 4.3 2.7
AT1G66080 2.7 2.2
AT2G42560 11.7 4.9
b
MYC2_DAP
Peaks count
Distance to TSS (bp)
g
ZF14 2.8 3.3
WRKY6 3.2 3.4
WRKY53 3.0 2.8
WRKY28 3.0 2.8
SAG21 14.1 16.1
SAG20 2.4 2.4
PLL4 4.1 3.5
DMR6 2.6 2.4
DML3 6.2 5.4
TIFY10B 20.3 22.9
RAP2.6 5.5 6.3
JAZ5 6.0 5.3
ILL6 2.8 2.8
PROPEP1 4.0 3.8

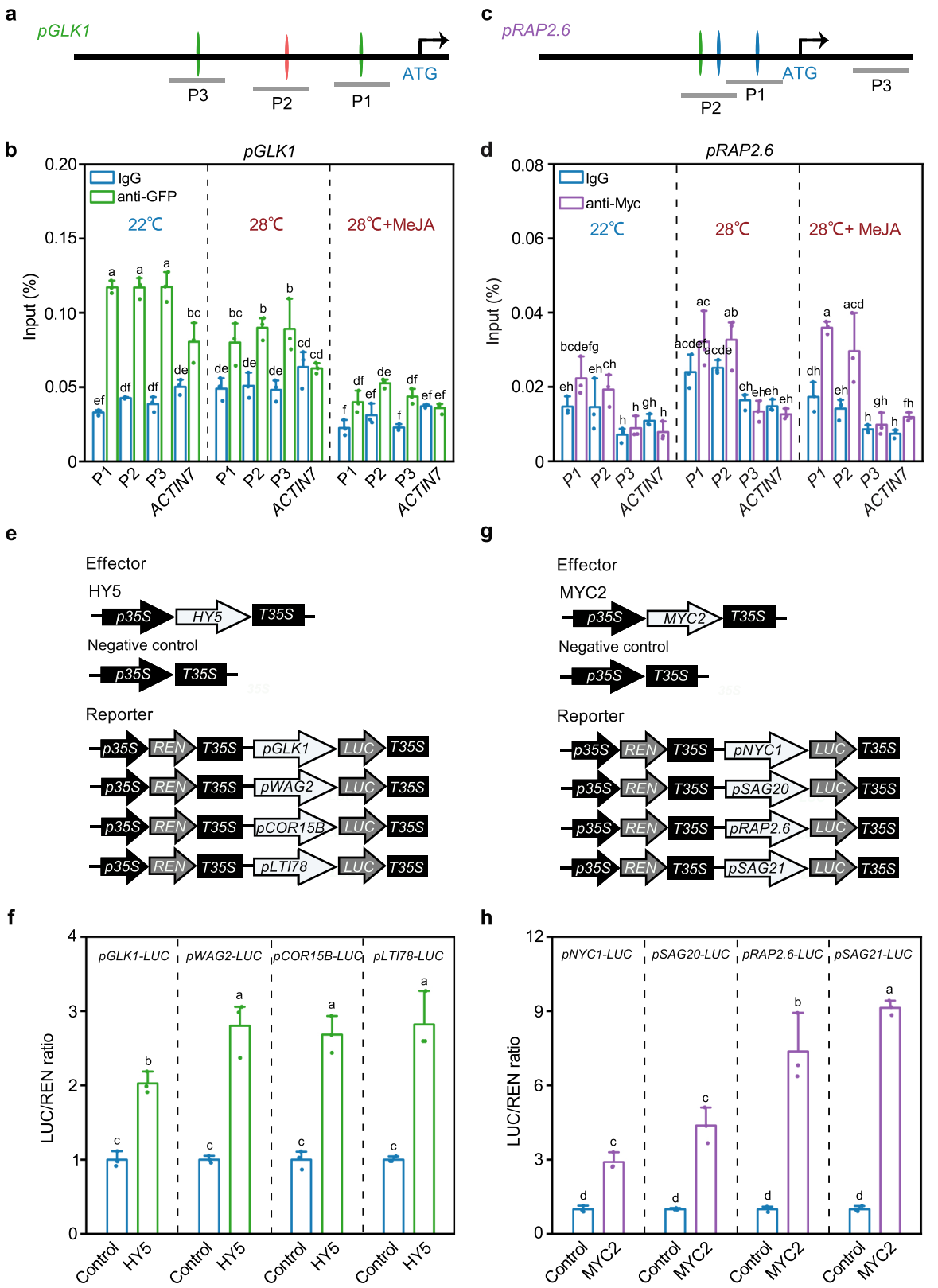
a
pGLK1
ATG
P3
P2
P1
c
pRAP2.6
ATG
P2
P1
P3
b
pGLK1
IgG
anti-GFP
22℃
28℃
28℃+MeJA
Input (%)
0.20
0.15
0.10
0.05
0
P1
P2
P3
ACTIN7
d
pRAP2.6
IgG
anti-Myc
22℃
28℃
28℃+ MeJA
Input (%)
0.08
0.06
0.04
0.02
0
e
Effector
HY5
p35S
HY5
T35S
Negative control
p35S
T35S
Reporter
p35S
REN
T35S
pGLK1
pWAG2
pCOR15B
pLTI78
LUC
T35S
g
Effector
MYC2
p35S
MYC2
T35S
Negative control
p35S
T35S
Reporter
p35S
REN
T35S
pNYC1
pSAG20
pRAP2.6
pSAG21
LUC
T35S
f
pGLK1-LUC
pWAG2-LUC
pCOR15B-LUC
pLTI78-LUC
LUC/REN ratio
4
3
2
1
0
Control
HY5
h
pNYC1-LUC
pSAG20-LUC
pRAP2.6-LUC
pSAG21-LUC
LUC/REN ratio
12
9
6
3
0
Control
MYC2